Initial Survey of the Wave Distribution Functions for Plasmaspheric Hiss Observed by ISEE I • F Lsrsvvgs 2 M PARROT, 2 L CAm6 •

L.R.O. Storey, François Lefeuvre, Michel Parrot, R R Anderson, L. Cairo

JOURNAL OF GEOPHYSICAL RESEARCH, VOL. 96, NO. A11, PAGES 19,469–19,489, NOVEMBER 1, 1991

Initial Survey of the Wave Distribution Functions for Plasmaspheric Hiss Observed by ISEE 1

L. R. O. STOREY,[1] F. LEFEUVRE,[2] M. PARROT,[2] L. CAIRÓ,[3] AND R. R. ANDERSON[4]

Multicomponent ELF/VLF wave data from the ISEE 1 satellite have been analyzed with the aim of identifying the generation mechanism of plasmaspheric hiss, and especially of determining whether it involves wave propagation on cyclic trajectories. The data were taken from four passes of the satellite, of which two were close to the geomagnetic equatorial plane and two were farther from it; all four occurred during magnetically quiet periods. The principal method of analysis was calculation of the wave distribution functions. The waves appear to have been generated over a wide range of altitudes within the plasmasphere, and most, though not all, of them were propagating obliquely with respect to the Earth's magnetic field. On one of the passes near the equator, some wave energy was observed at small wave normal angles, and these waves may have been propagating on cyclic trajectories. Even here, however, obliquely propagating waves were predominant, a finding that is difficult to reconcile with the classical quasi-linear generation mechanism or its variants. The conclusion is that another mechanism, probably nonlinear, must have been generating most of the hiss observed on these four passes.

1. INTRODUCTION

Plasmaspheric hiss is a broad-band and structureless extremely-low-frequency (ELF) electromagnetic emission that is almost always present in the Earth's plasmasphere and is commonly observed by magnetospheric satellites [*Taylor and Gurnett*, 1968; *Dunckel and Helliwell*, 1969; *Russell et al.*, 1969, 1972; *Muzzio and Angerami*, 1972; *Kelley et al.*, 1975; *Parady et al.*, 1975; *Cornilleau-Wehrlin et al.*, 1979]. However, in spite of these many observations, there is still no satisfactory theoretical explanation for its origin. Arguments have been given by *Thorne et al.* [1973] for amplification of natural incoherent emission by the Doppler-shifted electron cyclotron resonance instability, occurring in the equatorial region of the outer magnetosphere. This instability, however, is convective rather than absolute, so the generation mechanism envisioned, whether it be the original *Kennel and Petschek* [1966] mechanism or the self-consistent version developed by *Etcheto et al.* [1973], requires the existence at the equator of a continuous source of longitudinal waves, i.e., waves with their normals close to the direction of the magnetic field: oblique waves are not amplified because they suffer too much Landau damping.

Obviously the mechanism can be maintained by amplified waves that return to the source region after being reflected at the base of the ionosphere or after a magnetospheric reflection, so long as they return with their normals sufficiently close to the field to allow further amplification. This condition is likely to be met if the waves are generated inside field-aligned ducts, which guide them and keep their normals parallel to the field on the average [*Smith et al.*, 1960; *Smith*, 1961; *Helliwell*, 1965; *Gorney and Thorne*, 1980]. Indeed, hiss has been observed in association with large and intense ducts, both within the plasmasphere [*Koons*, 1989] and in regions detached from it [*Chan and Holzer*, 1976]; wave measurements made inside the ducts have confirmed that the normals are close to the direction of the magnetic field [*Hayakawa et al.*, 1986a; *Hayakawa*, 1987]. In theory, waves can also be guided on the inner edge of the plasmapause [*Inan and Bell*, 1977], and measurements made just inside the plasmapause, close to the magnetic equatorial plane, also have found approximately longitudinal propagation vectors [*Parrot and Lefeuvre*, 1986; *Hayakawa et al.*, 1986b, 1987]. Elsewhere in the plasmasphere, and especially at points remote from the equatorial plane, almost all of the hiss waves are propagating obliquely, so they cannot be in ducts [*Lefeuvre et al.*, 1983; *Hayakawa et al.*, 1986b].

Ray-tracing studies have shown that nonducted waves launched longitudinally at the magnetic equator tend to become oblique as they propagate away from it [*Aikyo and Ondoh*, 1971; *Huang and Goertz*, 1983]. Their normals are tilted toward the Earth by the general decrease of plasma density with increasing L and outward from the Earth by the decrease of magnetic field strength with increasing L, jointly with the effect of field line curvature. For a wave of arbitrary frequency launched from an arbitrary point on the equator, these competing effects are unlikely to cancel each other exactly: one or another will dominate, with the result that as the wave propagates, its normal becomes more and more inclined to the field, ultimately approaching the resonance cone.

Nevertheless, given a suitable distribution of the magnetospheric plasma, it is possible to find some particular wave frequencies and launch points for which these competing effects do indeed cancel, on the average, over a ray path out from the magnetic equatorial plane and back. Such paths involve a magnetospheric reflection and usually a reflection from the plasmapause as well, following which the wave returns to the equator with its normal again parallel to the field, though now directed into the opposite hemisphere; also, in general, it is now at a point different from its launch

[1]National Space Science Data Center, NASA Goddard Space Flight Center, Greenbelt, Maryland.
[2]Laboratoire de Physique et Chimie de l'Environnement, Centre National de la Recherche Scientifique, Orléans, France.
[3]Physique Mathématique Modèlisation et Simulation, Centre National de la Recherche Scientifique, Orléans, France.
[4]Department of Physics and Astronomy, University of Iowa, Iowa City.

Paper number 91JA01828.
0148-0227/91/91JA-01828$05.00

point. If the propagation continues, however, and if the plasma distribution is symmetrical with respect to the equator, then the part of the path in the second hemisphere is the mirror image of the part in the first, and the wave returns to its launch point with its normal once more parallel to the field. These paths are known as "cyclic trajectories", since waves launched onto them cycle around them indefinitely.

Cyclic trajectories were first described by *Thorne et al.* [1979], who suggested that wave propagation and the plasmapause may be important factors in the origin of plasmaspheric hiss. They pointed out that waves propagating on cyclic trajectories ("cyclic waves") would return to the equatorial growth region with field-aligned propagation vectors and thus experience further amplification. If the gain for one complete pass around the trajectory exceeded unity, then the system would be unstable overall, as in a laser or maser; i.e., it would act as a generator, not merely as an amplifier, of waves, which presumably would grow until limited by quasi-linear effects as in the original theory of *Kennel and Petschek* [1966]. Thorne et al. suggested that this process, which has also been described by *Lyons and Williams* [1984], would be particularly important for the maintenance of hiss during magnetically quiet periods, when a single transit through the growth region is insufficient to amplify the background incoherent cyclotron noise to detectable levels. On cyclic trajectories, with multiple transits through this region, the near-perfect reflection of wave energy would permit incoherent background noise to be amplified to observable levels even during weak gain conditions, thus accounting for the persistence of quiet time hiss.

The principal aim of the work described in the present paper was to test this theory of the origin of plasmaspheric hiss. Among the various features of cyclic waves, one in particular lends itself to experimental test, namely the fact that their normals are approximately parallel to the magnetic field at the equator. The theory predicts that measurements of the wave normal directions for plasmaspheric hiss, made in the magnetic equatorial plane under quiet conditions, should find the strongest waves propagating in directions close to the field.

Wave data for checking this prediction came from the ISEE 1 satellite and were selected on the basis of the following physical criteria. First, they were taken during magnetically quiet periods: the magnetic disturbance index K_p was less than 3 during at least the three previous days. Second, they were taken on satellite passes close to the magnetic equatorial plane; for comparison, some data taken far from this plane were examined as well. Specifically, we analyzed hiss data acquired by the ISEE 1 satellite on two passes close to the magnetic equatorial plane, called passes I and II, and two well away from this plane, called passes III and IV. Table 1 lists the position of the satellite together with the properties of the ambient plasma, at the start and finish of the part of each pass from which the wave data were taken. The final criterion was that electron density data, which are needed for the analysis of the wave data, should also be available out to and beyond the plasmapause, so that the position and intensity of the plasmapause could be determined.

These electron density data also were required in connection with another possible test of the importance of the plasmapause for the generation of plasmaspheric hiss. During long periods of magnetic quiet, the plasmapause recedes far from the Earth and can become indistinct, even to the point of being undetectable [*Chappell*, 1972]; for, instance, in Figure 6 of Chappell's paper the daytime electron density profile shows no sign of a plasmapause out to its upper limit at $L = 9$, though it becomes increasingly irregular beyond about $L = 6$. Under such conditions the plasmapause would be unable to reflect whistler mode waves, so the hiss should cease if it can only be generated on cyclic trajectories. This is, however, a weaker prediction than the one concerning the wave normal directions, since the hiss might also cease through a shortage of the energetic electrons required to sustain the instability.

Accordingly, our analysis of the wave data was mainly concerned with determining the wave normal directions. In view of the highly incoherent character of plasmaspheric hiss, this cannot be done well by the classical methods based on the plane wave approximation [*Thorne et al.*, 1973]. On the other hand the wave distribution function (WDF) method [*Storey and Lefeuvre*, 1979, 1980; *Lefeuvre and Delannoy*, 1979; *Lefeuvre et al.*, 1981; *Delannoy and Lefeuvre*, 1986; *Storey*, 1989], in which the observed electromagnetic field is assumed to be random, is entirely appropriate to such phenomena. It involves describing the field by a function $F(\omega, \kappa)$, called the WDF, which specifies how the electromagnetic wave energy density is distributed with respect to the angular frequency ω and to the direction of propagation characterized by the unit vector $\kappa = \mathbf{k}/|\mathbf{k}|$, with $\mathbf{k}$ the wavenumber vector. The field is supposed to be statistically stationary in time, and the medium homogeneous over dis-

TABLE 1. Details of the Four Passes Studied

		UT	MLT	MLAT	L	f_p	f_{ce}	Range of f/f_{ce}
Pass I (Jan. 16, 1977)	Start	1418	8.3	3.7	4.9	119	7.7	0.013–0.61
	Finish	1521	9.8	−11.9	2.4	322	74.5	0.001–0.06
Pass II (Dec. 9, 1977)	Start	0800	10.8	−4.1	6.1	90	4.0	0.025–1.18
	Finish	0909	11.7	−13.6	3.9	214	19.3	0.005–0.24
Pass III (Sept. 5, 1978)	Start	0934	16.2	−31.5	8.0	27.4	6.1	0.017–0.77
	Finish	1103	18.8	−50.3	6.4	120	94.7	0.001–0.05
Pass IV (Sept. 5, 1978)	Start	1217	7.4	54.0	6.9	109	99.2	0.001–0.05
	Finish	1355	11.8	46.8	10.5	13.4	5.2	0.019–0.90

From left to right, the successive columns contain the pass number and date, the event (start or finish of the pass), universal time, magnetic local time (hour), magnetic dipole latitude (degrees), L value, plasma frequency (kHz), electron gyrofrequency (kHz), and range of f/f_{ce} where f is the observed wave frequency.

tances greater than all the wavelengths involved. If these conditions hold, then the WDF can be determined, though with limited directional resolution.

As input data, WDF analysis requires simultaneous measurements of several components of the electromagnetic wave field. On ISEE 1 these and other data were provided by the University of Iowa plasma wave instrument [*Gurnett et al.*, 1978], which in certain modes of operation measured five field components simultaneously: two electric components on two radial electric dipole antennas with tip-to-tip lengths of 215 m and 73.5 m, and three magnetic components on a set of triaxial search coil antennas. The five signals could be connected to various electronic systems: the narrow-band sweep frequency receiver enabled us to visualize all the waves present in the 0.1- to 400-kHz band; two high-time-resolution spectrum analyzers, one covering the band from 5.6 Hz to 10 kHz and the other covering the band from 5.6 Hz to 311 kHz, gave us the instantaneous and averaged field strengths in 14 and 20 preassigned channels, respectively. The wave normal analyzer (WNA) measured the amplitudes and relative phases of the various electric and magnetic field components at the output of narrow-band filters, and these were the data that we used for the WDF analysis.

The WNA had the following characteristics: the bandwidth was 10 Hz, and the central frequency f was commanded to step, at a cadence of one step every 32 s, through 32 fixed frequencies spaced nonuniformly (more or less logarithmically) from 100 Hz to 5 kHz. The last column in Table 1 lists the corresponding range of the normalized frequency f/f_{ce}, where f_{ce} is the electron cyclotron frequency, or gyrofrequency. Assuming that the only ions present are protons, the lower hybrid frequency f_{lh} is such that $f_{lh}/f_{ce} \simeq 0.023$ so long as $f_p \gg f_{ce}$, which was true in most cases. For the purposes of our analysis, the WDFs are considered to be independent of frequency in the 10-Hz bandwidth; therefore in the function $F(\omega, \kappa)$ the components of the κ vector are the only variables.

The plan of the paper is as follows: in section 2 the broad characteristics of the observed plasmaspheric hiss are studied, in the light of a preliminary analysis concerning the frequency-time spectra, the autopower spectra, and the polarization of the waves; in section 3 our method for determining the WDF is briefly summarized, and the results of its application are presented; section 4 gives some statistics on the wave normal directions corresponding to the peaks of the WDFs; section 5 contains a theoretical ray tracing of the propagation paths of ELF waves in the plasmasphere during pass II; in section 6 the question of the generation mechanism of plasmaspheric hiss is discussed in the light of our experimental and theoretical findings and of related work by others. Finally our conclusions are given in section 7. This paper is an amplification of an earlier report by *Lefeuvre et al.* [1983]; a preview of some of the findings has been given by *Storey* [1989].

2. Preliminary Analysis

Before proceeding to the calculation of the WDFs, a preliminary analysis was performed in order to determine some of the more familiar characteristics of the waves present in the data. These comprised their frequency-time spectra, their autopower spectra, and various measures of their degree of polarization.

2.1. *Frequency-Time Spectra*

These are synoptic plots of short-term autopower spectra of one component of the electromagnetic field, the electric component measured by the 215-m dipole antenna. They were made by recording the output of the narrow-band sweep frequency receiver on film, as a shade of grey, in a rectangular area with frequency up the vertical axis and time along the horizontal axis. The spectrograms for passes I and II are presented in Figures 1 and 2, respectively; passes III and IV are displayed similarly in Figure 3. For each pass, vertical arrows indicate the time interval for which the wave data have been analyzed in detail. A line has been drawn at the local electron gyrofrequency calculated from the output of the magnetometer on board.

On all four passes, natural emissions are present at low frequencies. They are represented by the large grey area in the lower part of each figure. A mottled grey corresponds to chorus, a uniform grey to hiss. The emissions are mainly of the chorus type outside the plasmasphere and of the hiss type inside; however, chorus bands are also observed well inside the plasmasphere. Note that the hiss band has an upper cutoff frequency which for the equatorial passes (Figures 1 and 2) is at approximately half the local electron gyrofrequency, as some previous workers have found [*Dunckel and Helliwell*, 1969; *Huang et al.*, 1983]. For the off-equatorial passes (Figure 3), the hiss band is less well structured; it would be interesting to know whether this is true in general, since it is germane to the question of the range of L values over which the hiss is generated. Dunckel and Helliwell, who analyzed a large body of wave data from OGO 1, taken during a magnetically quiet period in the range $2.5 \leq L \leq 13$ and covering $\pm 50^\circ$ of geomagnetic latitude, found that the upper frequency limit of most of the emissions, both hiss and chorus, was proportional to the minimum electron gyrofrequency along the magnetic field line passing through the satellite, i.e., to the gyrofrequency at the equator; the factor of proportionality usually lay between 0.2 and 0.6, with a median value of ~ 0.45. Other authors, however, report that the power and the frequency spectra of the hiss waves show little variation with L; see *Lyons and Williams* [1984] and the references therein.

Natural emissions are also present at high frequencies, above the gyrofrequency. They are represented by the grey area extending from the top of the figure down to a sharp lower limit where they are particularly intense. This lower cutoff is believed to correspond to the upper hybrid resonance of the ambient plasma [*Mosier et al.*, 1973; *Gurnett et al.*, 1979]. Thus from measurements of the cutoff frequency, and knowing the local gyrofrequency, it is possible to determine the plasma frequency and hence the ambient electron density. Densities determined in this way have been compared with those from the relaxation sounder on ISEE 1 [*Harvey et al.*, 1978, 1979], and generally they agreed within a few percent.

By examining how the upper hybrid frequency varies with time on a frequency-time spectrogram and knowing the satellite orbit, it is often possible to locate the plasmapause. On pass I the inner edge of the plasmapause is at $L \simeq 7.7$, while it is at $L \simeq 8.2$ on pass II; in view of the low magnetic activity ($K_p < 3$ during at least the three previous days) and of the magnetic local time (see Table 1), it is not surprising that these L values are so large and that the signature of the plasmapause is less distinct than in the examples shown by

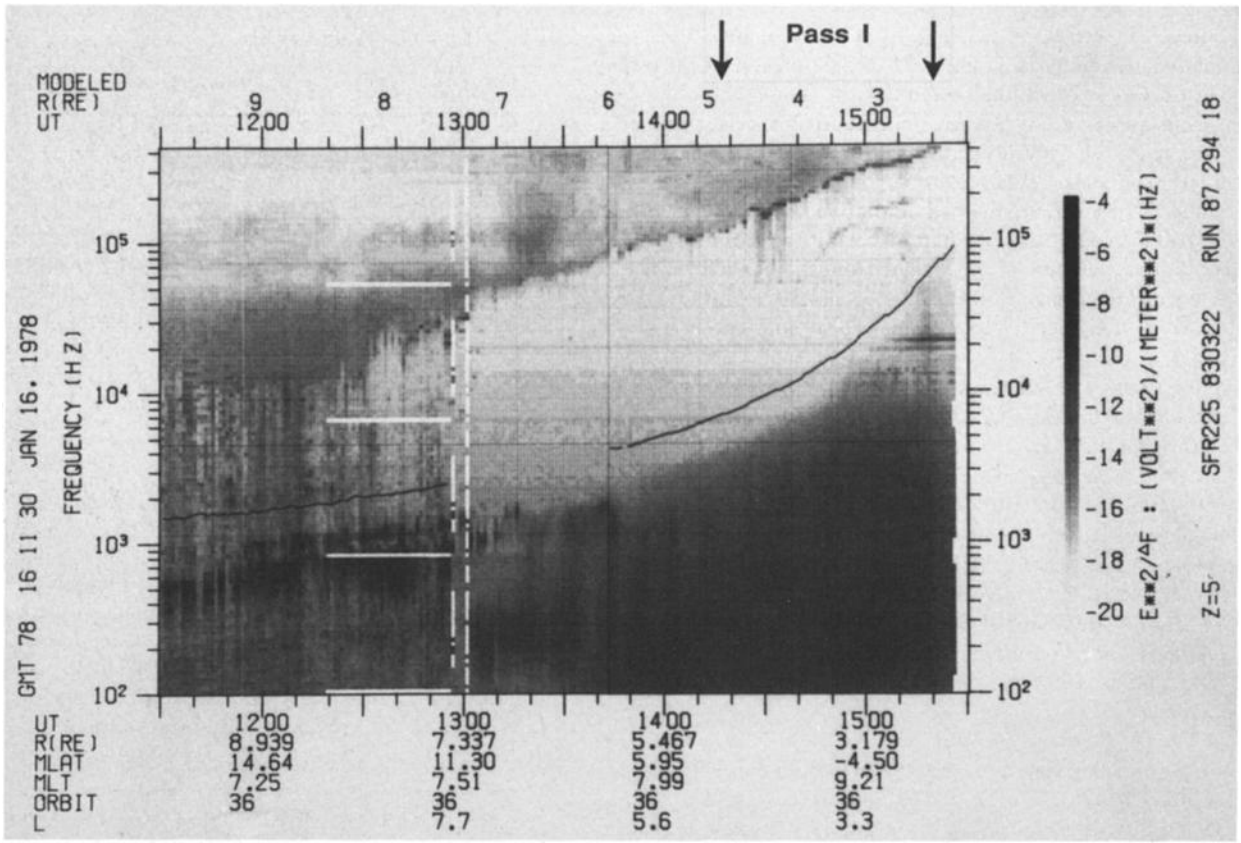

Fig. 1. Frequency-time spectrogram for orbit 36 on January 16, 1978. The six quantities tabulated below it are (from top to bottom), universal time, radial distance from the center of the Earth (in Earth radii), magnetic dipole latitude, magnetic local time, orbit number, and L value.

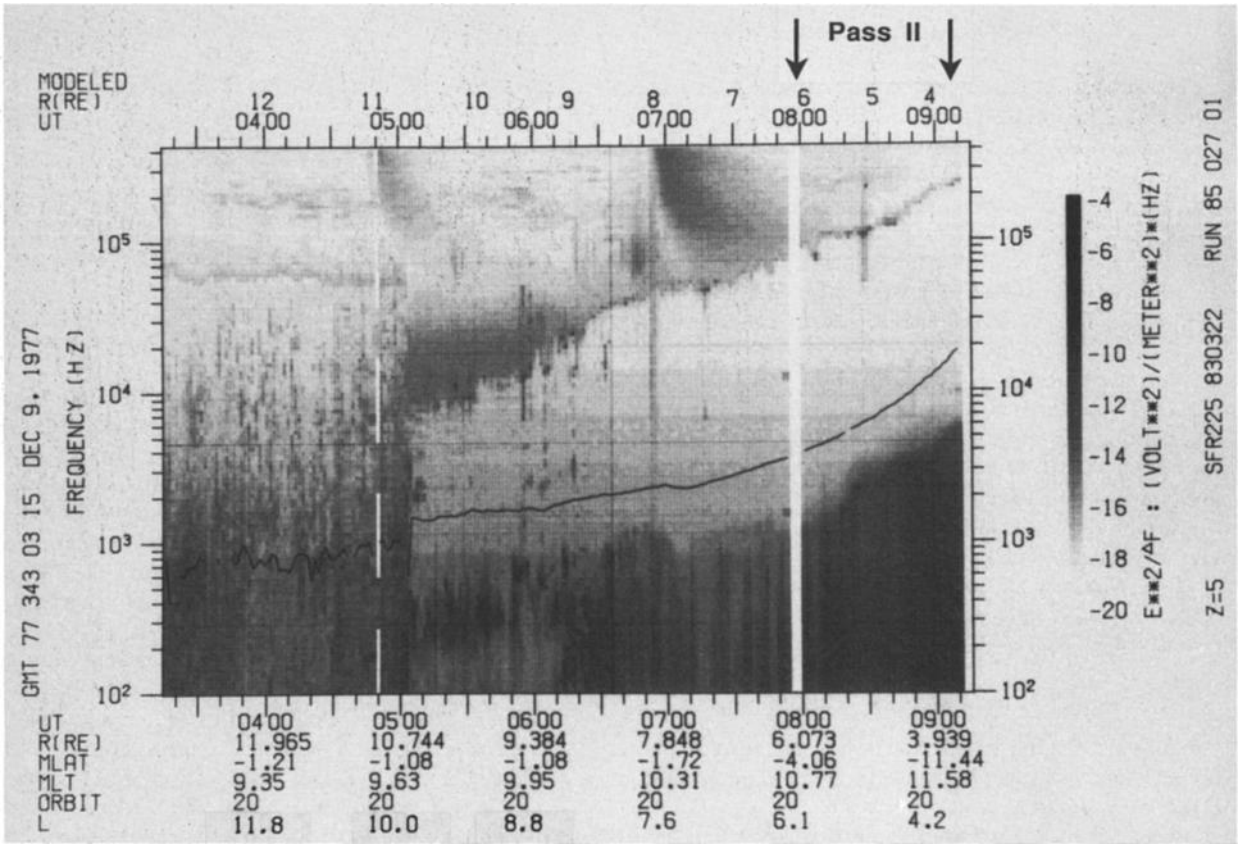

Fig. 2. Frequency-time spectrogram for orbit 20 on December 9, 1977.

Gurnett et al. On passes III and IV, however, the position of the plasmapause cannot be identified, and in fact there does not seem to be one; hence it is doubtful whether, on this occasion, wave reflection from the plasmapause could have played any part in the generation of hiss, which was present nonetheless.

Figure 1 seems to show a possible second plasmapause at roughly 1230 UT, which may be evidence of a detached plasma region [*Taylor et al.*, 1970; *Chappell et al.*, 1970]. Features of this kind are fairly common in the frequency-time spectra from ISEE 1.

2.2. *Autopower Spectra*

Power spectra of the total magnetic field, obtained by summing those of its three axial components, have been constructed from the WNA outputs for all four passes. The spectra for pass I are graphed in Figure 4; the corresponding L values are listed in the caption. A spectrum has been constructed for every frequency sweep, excepting the ones that for technological reasons such as poor telemetry data are very incomplete. Our objectives in examining these data were, first, to check that the observed spectra were consistent with those previously reported for ELF hiss and, second, to see whether they were particularly intense on certain parts of the satellite orbits, which might then be identified tentatively with traverses of source regions for the waves.

On pass I (Figure 4) the highest power spectral densities, exceeding $10^{-4}\ \gamma^2$/Hz, occur at the bottom of the observed frequency range. Three out of the four spectra decrease more or less monotonically with increasing frequency, the exception being the spectrum for sweep 1, where there is a peak at 1200 Hz due to a band of chorus. Though much less intense, chorus activity is still perceptible on sweep 2, at a slightly higher frequency. Apart from such details, the spectra for sweeps 2, 3, and 4 are of similar shape, but the intensity is greatest on sweep 3. Since the satellite is close to the magnetic equator (the magnetic dipole latitude (MLAT) varies from $-2.5°$ to $-6°$ during sweep 3), this enhancement suggests that it may then be near the center of a broad source region, which it is entering and leaving on sweeps 2 and 4, respectively.

The spectra for passes II–IV are broadly similar to those on pass I, though the power spectral densities of the emissions are mostly weaker than on pass I. In particular, for the off-equatorial passes III and IV the power below 400 Hz is generally much less than it is during passes I and II.

The broad features of these spectra agree with earlier reports [*Dunckel and Helliwell*, 1969; *Russell et al.*, 1972; *Muzzio and Angerami*, 1972]. Some questions as to which details are significant will be discussed later, in conjunction with the results of the WDF analysis.

2.3. *Polarization*

As groundwork for the WDF analysis, the spectral matrix of the five-component field data had to be calculated, and various quantities related to the polarization of the waves were obtained as by-products. They measure the extent to which the polarization is a pure state, i.e., to which the field resembles that of a plane wave in one of the two magnetoionic modes, here the whistler mode.

At each frequency step f_0 the WNA yields measurements of the amplitudes and of the relative phases of the electric

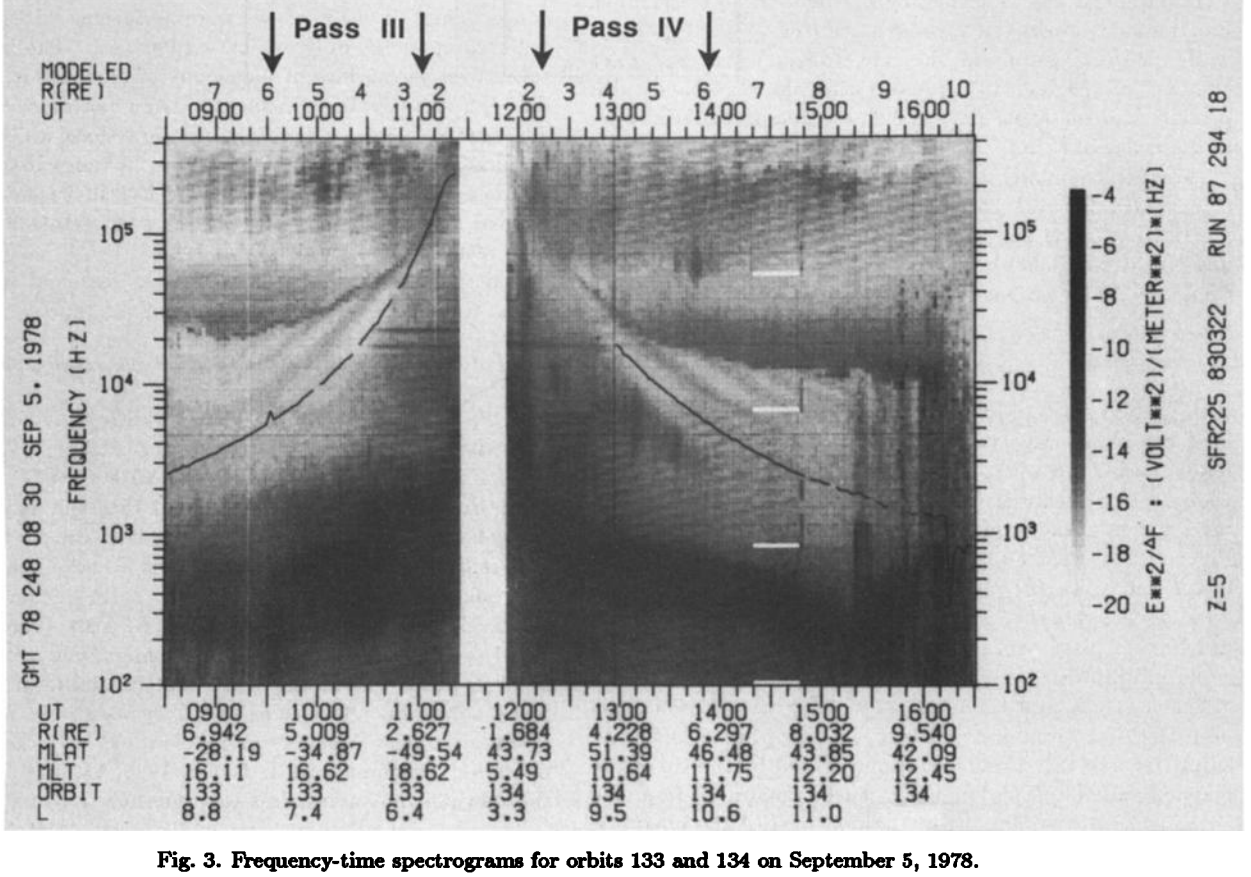

Fig. 3. Frequency-time spectrograms for orbits 133 and 134 on September 5, 1978.

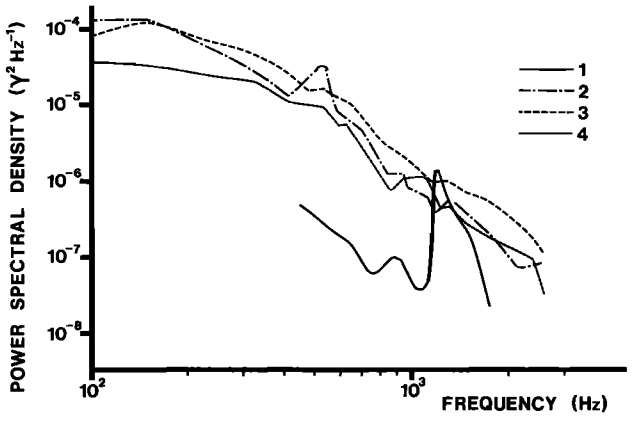

Fig. 4. Autopower spectra of the total magnetic field for four consecutive sweeps during pass I, corresponding to the following approximate L values: (1) 4.9–4.3; (2) 4.3–3.6; (3) 3.6–2.9; (4) 2.9–2.4.

and magnetic wave field components. For the sake of simplicity a generalized electric field vector $\mathcal{E}$ with five components is defined. It is written

$$\mathcal{E}_{1,2} = E_{x,y} \qquad \mathcal{E}_{3,4,5} = cB_{x,y,z} \tag{1}$$

with E_x, E_y and B_x, B_y, B_z the components of the electric field and magnetic induction vectors of the wave field, measured in the frame of reference of the satellite, while c is the speed of light. The five components of $\mathcal{E}$ are measured in a band of width $\Delta f = 10$ Hz centered on some frequency f_0, a time $T = 32$ s being spent at each frequency. From their time-averaged autopowers and cross-powers, the values of their spectral matrix elements S_{ij} at the frequency f_0 are estimated in the way described by *Lefeuvre and Storey* [1977]. For the autopowers the variances are $\langle(\delta S_{ii})^2\rangle \simeq S_{ii}^2/T\Delta f$, while for the cross-powers they are $\langle(\delta S_{ij})^2\rangle \leq S_{ii}S_{jj}/T\Delta f$ [*Bendat and Piersol*, 1971]; in our case, the time-bandwidth product had the value $T\Delta f \simeq 320$, so the uncertainties were of the order of $(T\Delta f)^{-1/2} \simeq 6\%$.

A degree of polarization can be estimated from the three eigenvalues $\lambda_1, \lambda_2, \lambda_3$ of the magnetic part of the spectral matrix, i.e., from the nine elements that involve the magnetic field components alone. Following equation (34) of *Samson* [1977], we have defined the degree of polarization as

$$p = \lambda_1/(\lambda_1 + \lambda_2 + \lambda_3) \tag{2}$$

with $\lambda_1 > \lambda_2 > \lambda_3$. It tends toward unity when the signal is of the plane wave type (e.g., very coherent chorus) and tends toward 1/3 when the wave energy is distributed over a wide angular spectrum (e.g., hiss). On pass I, for instance, it takes values of the order of 0.96 in the chorus band visible in Figure 1 at the plasmapause ($L \simeq 7.7$) and of the order of 0.4 to 0.7 well inside the plasmapause ($L < 5$). At intermediate L values the values of p range from 0.6 to 0.7, indicating the presence of hissy chorus, for which our method of analysis is inappropriate.

When it appears from the value of p that the wave is perfectly or approximately plane, it is helpful to know the ellipticity e of the variance ellipsoid traced by the tip of the magnetic vector. This quantity can be computed from the eigenvalues μ_1, μ_2, and μ_3 of the real part of the magnetic spectral matrix [*McPherron et al.*, 1972], by the relation

$$e^2 = \mu_2/\mu_1 \tag{3}$$

with $\mu_1 > \mu_2 > \mu_3$. It is equal to zero for linear polarization and to unity for circular polarization. In the whistler mode it is expected to vary between 0.95 (oblique propagation) and 1.0 (longitudinal propagation) for perfectly plane waves. The values generally obtained here (0.80 to 0.95) confirm that the waves are being propagated in the whistler mode with a slight spread in the κ vectors, i.e., they are only approximately plane.

3. WDF Analysis

3.1. *Method*

We adopt a Cartesian coordinate system $Oxyz$ in which the Oz axis is parallel to the Earth's magnetic field $\mathbf{B}_0$, the Ox axis is in the local magnetic meridian plane pointing toward lower L shells, and the Oy axis is oriented westward. In this system the κ vector is characterized by the polar angle θ that it makes with $\mathbf{B}_0$ and by the azimuthal angle ϕ, the origin of which is the Ox axis. The WDF is a function of these two angles and of the frequency. For convenience it is written $F(\omega_0, \cos\theta, \phi)$ at the angular frequency $\omega_0 = 2\pi f_0$ [*Storey and Lefeuvre*, 1980].

The WDF is related to the spectral matrix element by the set of integral equations

$$S_{ij}(\omega_0) = \frac{\pi}{2} \oint a_{ij}(\omega_0, \cos\theta, \phi)\, F(\omega_o, \cos\theta, \phi)\, d\sigma \tag{4}$$

where i and j run from 1 to $n \leq 6$, where n is the number of field components used in the analysis. In the present instance, $n \leq 5$ since ISEE 1 measured only five out of the six components of the electromagnetic wave fields. However, we were unable to exploit the data for the two electric components, so our analyses were performed with the magnetic components only, hence with $n = 3$. The integral is taken over the surface of the sphere of unit radius, of which $d\sigma = |d(\cos\theta)\, d\phi|$ is an element [*Storey and Lefeuvre*, 1979]. The kernels a_{ij} are known analytic functions which depend implicitly on the plasma parameters; in the whistler mode, at frequencies well above the lower hybrid frequency, they depend only on the electron plasma and cyclotron frequencies, respectively denoted f_p and f_{ce}.

Splitting up the equations (4) into real and imaginary parts, we obtain $N = n^2$ equations of the type

$$P_k(\omega_0) = \frac{\pi}{2} \oint q_k(\omega_0, \cos\theta, \phi)\, F(\omega_0, \cos\theta, \phi)\, d\sigma \tag{5}$$

with $P_1 = S_{11}$, $P_2 = \mathrm{Re}(S_{12})$, $P_3 = \mathrm{Im}(S_{12})$, ..., $P_{25} = S_{55}$ and with $q_1 = a_{11}$, $q_2 = \mathrm{Re}(a_{12})$, $q_3 = \mathrm{Im}(a_{12})$, ..., $q_{25} = a_{55}$. Here we have taken the case with $n = 5$, $N = 25$, as an example to illustrate the point that the quantities P and q have single indices, which, however, run up to double figures, whereas each of the quantities S and a has a pair of single-figure indices.

The determination of $F(\omega_0, \cos\theta, \phi)$ from the estimates $\hat{P}_k$ of the P_k values is an inverse problem, and moreover, it is an ill-posed one in the sense that it admits of infinitely many solutions. Here it is solved by using the maximum entropy concept [*Lefeuvre and Delannoy*, 1979; *Lefeuvre et al.*, 1981; *Delannoy and Lefeuvre*, 1986]. Briefly, we select the solution that maximizes the quantity

$$-\oint F(\omega_0, \cos\theta, \phi)\, \ln[F(\omega_0, \cos\theta, \phi)]\, d\sigma \tag{6}$$

It is

$$F(\omega_0, \cos\theta, \phi) = \exp\Big[-1 + \sum_{k=1}^{N^2} \lambda_k q_k(\omega_0, \cos\theta, \phi)\Big] \quad (7)$$

the Lagrangian multipliers λ_k being given, by an iterative process, values that minimize a quantity of the form

$$\frac{1}{N} \sum_{k=1}^{N} \frac{(\hat{P}_k - P_k)^2}{\langle(\delta \hat{P}_k)^2\rangle} \quad (8)$$

with $\langle(\delta \hat{P}_k)^2\rangle$ the variances of the $\hat{P}_k$. The minimization is pursued until this quantity becomes less than a certain limit, whereupon it is stopped. In the present work this limit was generally set at 1.64, corresponding to a 90% confidence interval for the averaged fit between the data $\hat{P}_k$ on the one hand and, on the other hand, the P_k computed from the maximum entropy model of the WDF by inserting (7) into (5) and evaluating the surface integrals.

Such solutions are often unstable, meaning that they are strongly modified by slight changes in the data; indeed, this is the reason for not pursuing the minimization of (8) until this quantity vanishes. A major cause of instability is linear interdependence of the kernels q_k, and it can be cured, at the price of some loss of data, by orthogonalizing them and then eliminating some of the smallest ones [*Lefeuvre and Delannoy*, 1979; *Lefeuvre et al.*, 1981; *Delannoy and Lefeuvre*, 1986]. The wave distribution function F is then found by solving a reduced set of $M < N$ integral equations similar to (5), but with transformed kernels and data. The solution is found in the way outlined in the previous paragraph, except that the quantity to be minimized, which is similar to (8), involves a sum over only M terms instead of N; in our analyses, based on the magnetic field data alone, we generally took $M = 6$.

The validity of the solutions is assessed by means of a stability parameter Q and a prediction parameter P_r. The former is defined as the ratio of the mean-square error of the solution computed from the $\langle(\delta P_k)^2\rangle$ to the mean-square value of the solution itself. The latter, which is given by (8) as it stands (i.e., with N terms in the sum), characterizes the global discrepancy between the estimates $\hat{P}_k$ derived from the experimental data and the values P_k reconstructed from the solution; the extent to which it exceeds the value 1.64 is a measure of the amount of data lost in the effort to stabilize the solution.

The foregoing account of our method of analysis is a condensed and simplified one. More details are given in the referenced papers.

3.2. *Results*

WNA data for the hiss emissions observed during passes I to IV were analyzed systematically in terms of the WDF. The analysis was restricted to frequencies greater than twice the local lower hybrid frequency, so as to be able to neglect ion effects. Only solutions having $Q < 2$ and $P_r < 2$ will be discussed here. This rigorous data selection explains why so few sweeps are considered and why the data are so sparse for some of them.

Most of the WDFs obtained for chorus events in the outermost part of the plasmasphere have been found to be too unstable to be trusted, except perhaps for the most strongly polarized events ($p > 0.95$). In such cases, the signal-to-noise ratio appears to be high, despite the errors introduced by samples taken outside the chorus elements. The κ vector corresponding to the peak of the WDF has approximately the same direction for all the elements observed at any one time and is very oblique to the Earth's magnetic field.

For the purpose of the WDF analysis the coefficients a_{ij} (or q_k) have been calculated using the values of the electron plasma frequency derived from the electron density measurements made by the relaxation sounder on board ISEE 1 [*Harvey et al.*, 1978, 1979]; this value agreed with the one derived from the plasma wave experiment itself, by analyzing spectrograms such as those of Figures 1 to 3. The value of the electron gyrofrequency was obtained from the measurements of the on-board magnetometer.

Typical examples of the WDFs obtained on pass I from the magnetic data alone are displayed as contour lines on the polar diagrams in Figure 5. The scale of F is linear and runs from 0 to 10; contours are traced at the values 1, 3, 5, 7, and 9. The outer circle corresponds to $\theta = 90°$, while the inner circle indicates the position of the resonance cone for the whistler mode. This analysis, based only on the magnetic field components, cannot distinguish between two waves propagating in exactly opposite directions; the function evaluated is actually

$$\mathcal{F} \equiv F\Big(\omega_0, \cos\theta, \phi\Big) + F\Big(\omega_0, \cos(180° - \theta), \phi + 180°\Big) \quad (9)$$

and accordingly the diagrams cover only the range $0 \leq \theta \leq 90°$. On the other hand, the WDFs derived from the magnetic field components alone are less sensitive to errors in the determination of the ambient electron density, compared with those derived using electric field components as well.

In Figures 5a, 5b, and 5c the same WNA step (471 Hz) is observed at three different times about 17 min apart, on sweeps 1, 2, and 3, respectively. At 50% of the maximum value (level 5) the three WDFs are similar. The waves are very oblique ($80° < \theta < 85°$) and spread out in azimuth ($105° < \phi < 240°$ on sweep 1, and $120° < \phi < 270°$ on sweeps 2 and 3). The change in ϕ between sweeps 1 and 2 is not necessarily significant since it is of the order of the uncertainty in the WDF determination [*Lefeuvre et al.*, 1982]. Considering the solutions at 10% of the maximum value (level 1) we see that wave energy is present at almost all ϕ values; a secondary peak even appears at $\phi \simeq 30°$ on sweep 3.

WDFs obtained from three successive WNA steps on sweep 2, at higher frequencies, are presented in Figures 5d, 5e, and 5f. Again the wave energy is being conveyed by very oblique waves. However, there are two significant differences from the WDFs in the previous figures: first, the energy is shared almost equally between two distinct wave packets, and second, the θ values are slightly smaller than previously ($55° < \theta < 80°$ at level 5). Once more the shift in ϕ, particularly noticeable between Figures 5e and 5f, is not necessarily significant.

The WDFs for pass II are especially interesting, since they include cases of propagation mainly at small θ angles. These occur for values of the normalized frequency higher than those encountered on pass I, in particular for $0.2 < f/f_{ce} < 0.3$; an example is given in Figure 6. This phenomenon appears on sweeps 1 and 2: on sweep 3, unfortunately, the WDFs are unreliable at these frequencies.

On all four passes, most of the WDFs exhibit two peaks, though some have only one, while a few cases with three

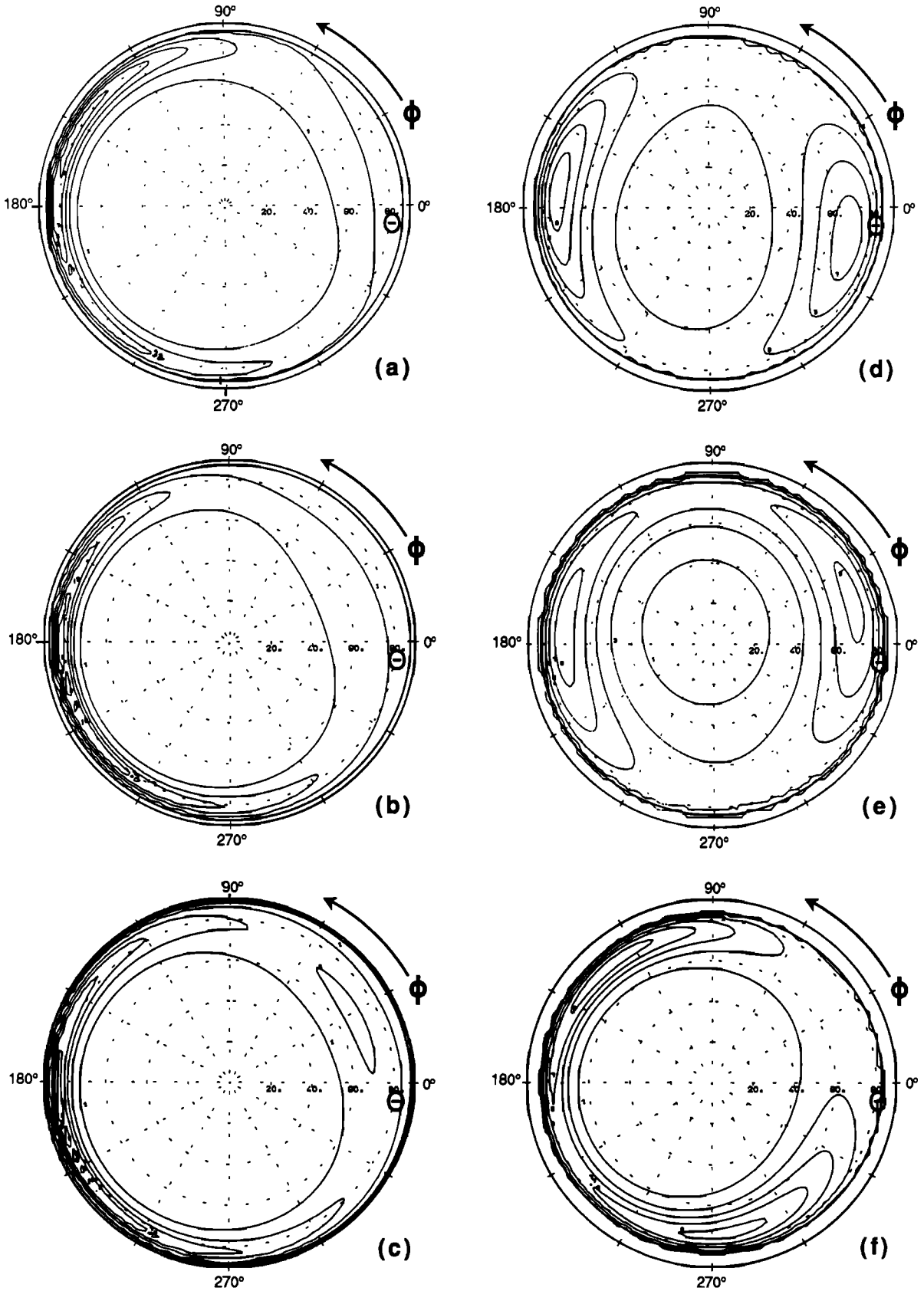

Fig. 5. Wave distribution functions for plasmaspheric hiss from pass I. In the column on the left, at the same frequency (471 Hz) but at different universal times: (a) 1418:31; (b) 1435:34; and (c) 1452:38. In the column on the right, at different frequencies but at almost the same UT: (d) 1299 Hz at 1443:02; (e) 1494 Hz at 1443:34; and (f) 1695 Hz at 1445:05.

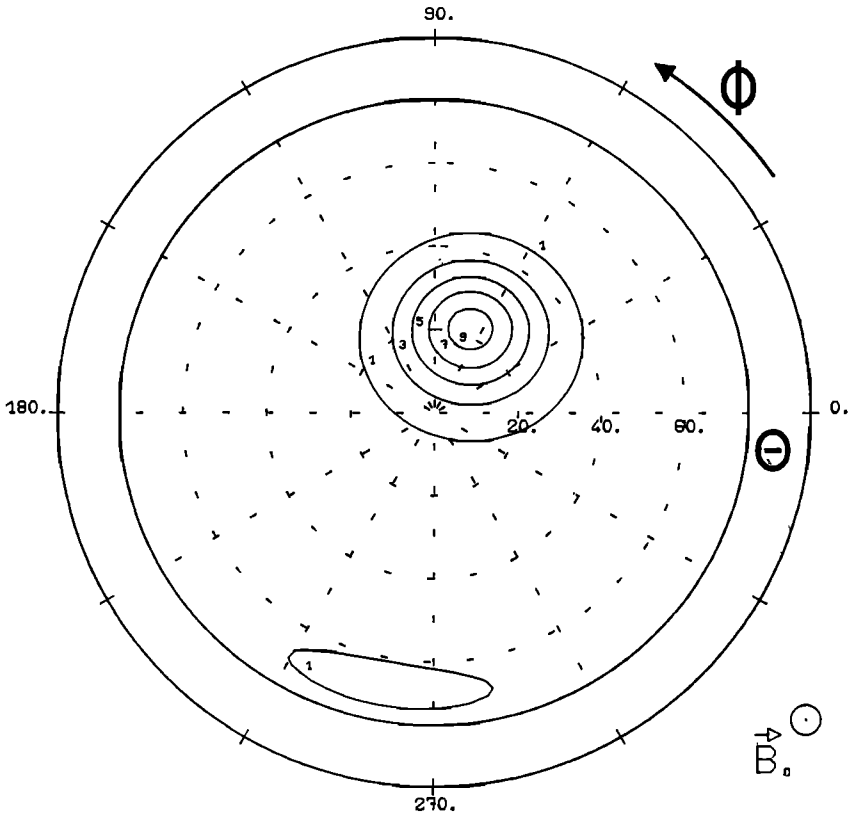

Fig. 6. WDF from pass II, at 1494 Hz and 0824:32 UT. The main peak has $\theta = 23°$.

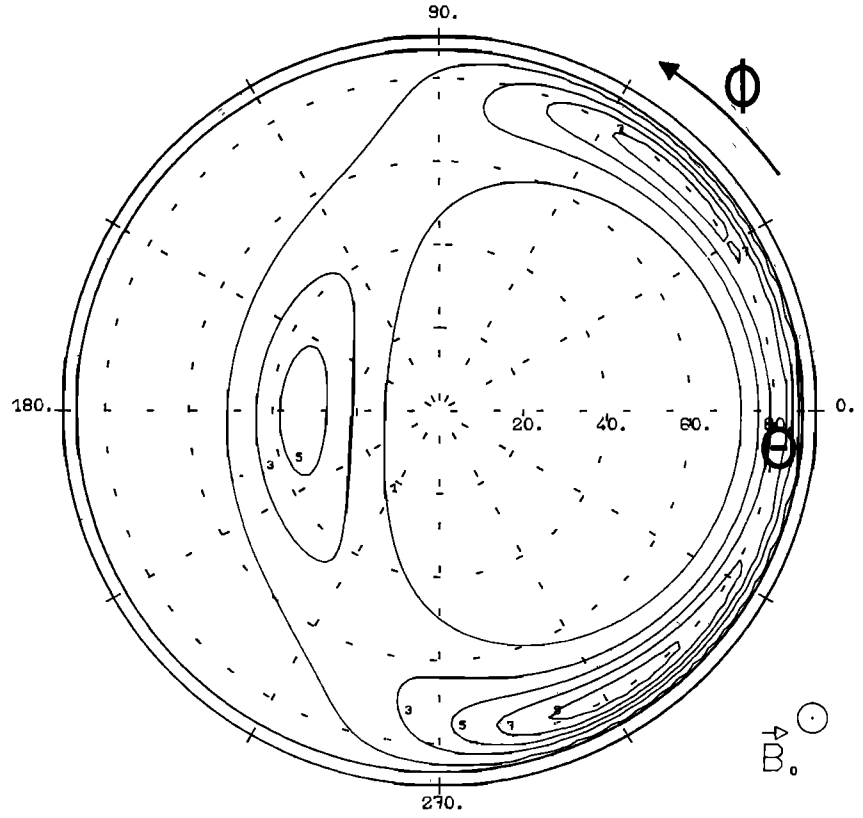

Fig. 7. WDF from pass IV, at 416 Hz and 1335:12 UT, showing three peaks.

were observed on pass IV (Figure 7). Defining a two-peaked WDF as one in which there is a secondary peak with an intensity at least equal to 20% of that of the main peak, we find that two-peaked WDFs occur in 56% of the cases on pass I, 60% on pass II, 42% on pass III, and 77% on pass IV.

From our analysis based only on the magnetic components of the wave field, we are unable to tell whether the component of κ parallel to $\mathbf{B_0}$ has the same or the opposite sign for the two peaks. In principle, this ambiguity could be resolved by analyzing the electric data as well, and we tried to do so, but unfortunately without success. Almost always, judging by their variances, both the real and imaginary parts of the cross-spectra between the electric and magnetic field components are statistically insignificant, even in respect of their signs, so no conclusion can be drawn from them. The only indication we have is that in the few cases where hiss events observed by GEOS 1 could be analyzed fully, it was found that both peaks of the WDF corresponded to waves propagating away from the equator [*Lefeuvre et al.*, 1981; *Lefeuvre and Helliwell*, 1985]; however, these GEOS 1 observations were made beyond the plasmapause. The fact that echoing whistlers and emissions have not been seen beyond the plasmapause is further evidence against the existence, in this region, of hiss waves propagating toward the equator [*Burtis and Helliwell*, 1976].

4. Wave Normal Directions

The waves of plasmaspheric hiss are widely spread in wave normal direction, as our WDF analysis has shown. Nevertheless, it has also shown that one or, more usually, two wave normal directions are preferred in the sense that they correspond to distinct maxima of wave energy density. The results concerning these preferred wave normal directions, i.e., the corresponding values of the angles θ and ϕ, will now be reviewed, after which the overall symmetry of the WDFs will be examined. Finally, a comparison will be made with earlier results from GEOS 1.

4.1. θ Values

The key parameter for understanding the propagation of whistler mode waves is the normalized frequency f/f_{ce}; the shape of the phase refractive index surface depends only on this parameter, so long as $f_p \gg f_{ce}$, which was almost always the case (see Table 1). Accordingly, the θ values for the peaks of the WDFs have been plotted versus f/f_{ce} for passes I to IV in Figures 8 to 11. The solid circles refer to the main peaks, and the open circles to the secondary peaks whenever these exist. The two curves are theoretical: the upper one is of the resonance angle θ_r, beyond which propagation is impossible ($\cos\theta_r \simeq f/f_{ce}$ when $f_p \gg f_{ce}$); the lower one is of the Gendrin angle θ_G [*Gendrin*, 1961], defined as the nonzero θ value at which the ray direction is parallel to the magnetic field ($\cos\theta_G \simeq 2f/f_{ce}$ when $f_p \gg f_{ce} > 2f$). At frequencies above $f_{ce}/2$, no Gendrin angle exists. Below $f_{ce}/2$ the ray has the same azimuth as the normal when $\theta < \theta_G$ and the opposite azimuth when $\theta_G < \theta < \theta_r$.

Figure 8 presents the data from the four successive WNA frequency sweeps on pass I. Most of the plotted points con-

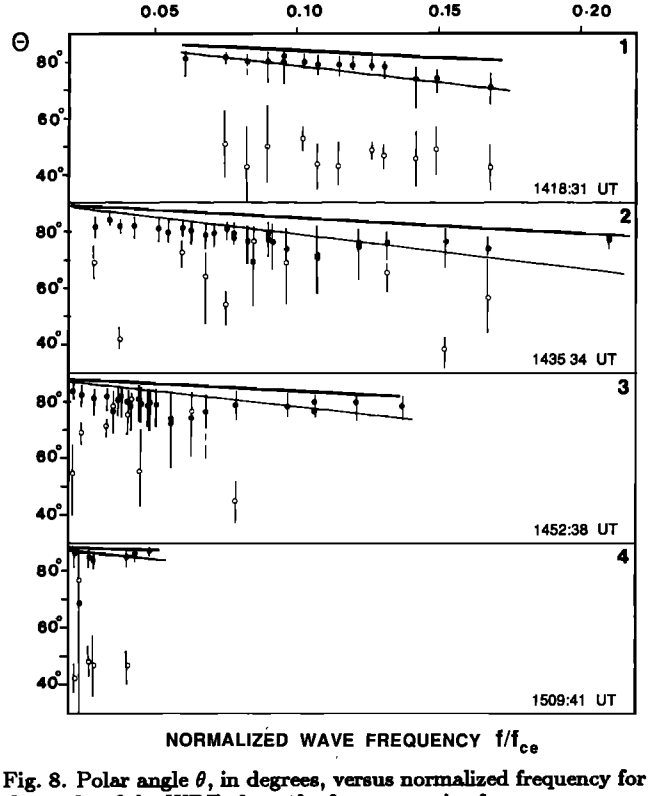

Fig. 8. Polar angle θ, in degrees, versus normalized frequency for the peaks of the WDFs from the four successive frequency sweeps on pass I. The solid circles represent the main peaks, and the open circles the secondary peaks. The bars give the widths of the peaks at half their heights. The start time for each sweep is marked in the lower right-hand corner of the corresponding panel.

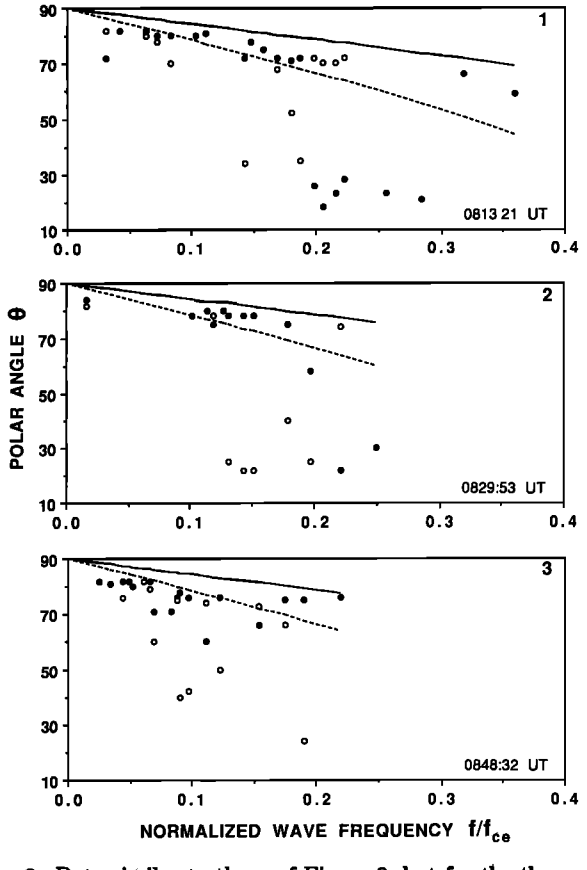

Fig. 9. Data similar to those of Figure 8, but for the three successive frequency sweeps on pass II.

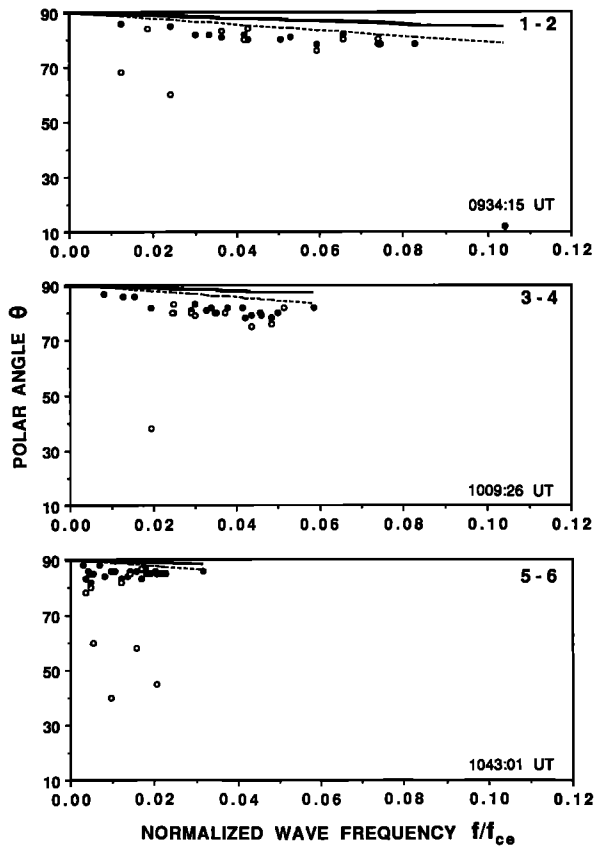

Fig. 10. Data similar to those of Figure 8, but for the three successive pairs of frequency sweeps on pass III: (top) sweeps 1 and 2 combined; (middle) sweeps 3 and 4 combined; and (bottom) sweeps 5 and 6 combined.

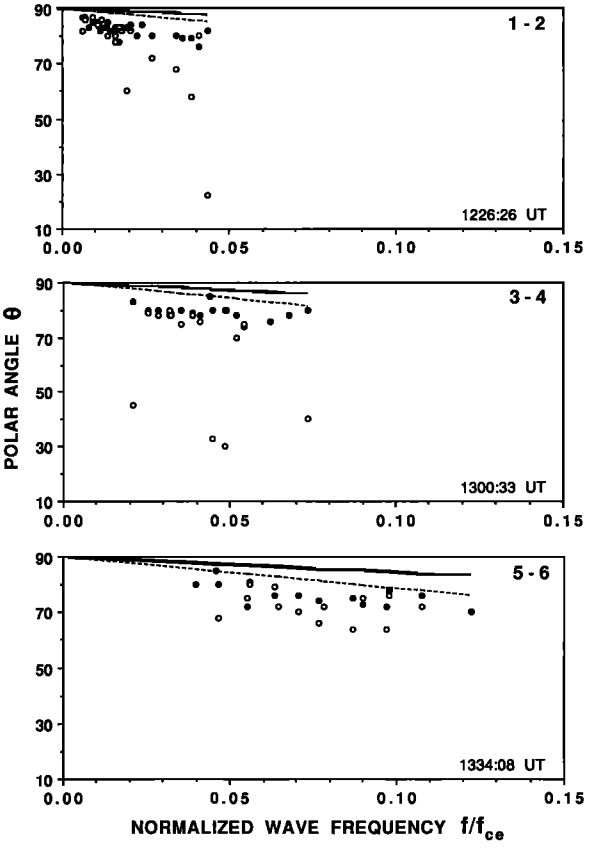

Fig. 11. Data similar to those of Figure 10, but for pass IV.

cern frequencies such that $f/f_{ce} < 0.2$: though data were obtained at higher frequencies, the inferred WDFs are of too poor quality to pass our selection criteria. Note that the vertical scales of θ begin at 30°. The vertical bar through each of the plotted points indicates the width of the WDF; its extremities are at the θ values where $\mathcal{F}$ equals half its value at the peak.

Examination of this figure reveals that on all four sweeps the propagation is mainly oblique. At $f/f_{ce} < 0.1$ the θ values for the main peak tend to be slightly below θ_G, while for $0.1 < f/f_{ce} < 0.2$ they are mostly between θ_G and θ_r. This is true even for sweep 3, which may correspond to a source region, as we have suggested on the evidence of its power spectrum (Figure 4). In the WDFs for all four sweeps, however, secondary peaks occur at lower θ values, mostly in the range 30°–60°.

The corresponding data from pass II are presented in Figure 9; here the widths of the peaks have not been plotted, but they are similar to those in Figure 8. The upper limit of normalized frequency, attained only on sweep 1, is $f/f_{ce} \simeq 0.35$. At $f/f_{ce} < 0.2$ the behavior of the data is similar to that noted previously for pass I, except that some secondary peaks occur at lower θ values, in the range 10°–30°. At $f/f_{ce} \simeq 0.2$, however, a marked change takes place: the main peak of the WDF now appears in this low range of θ, while a secondary peak persists between θ_G and θ_r up to $f/f_{ce} \simeq 0.22$ and then disappears. The six WDFs in the range $0.2 < f/f_{ce} < 0.3$ possess these features. At still higher normalized frequencies the previous behavior reasserts itself: the two WDFs at $f/f_{ce} > 0.3$ both exhibit single peaks between θ_G and θ_r. On sweep 2 also, the two WDFs at $f/f_{ce} > 0.2$ have single peaks with $\theta < 30°$, but unfortunately no WDFs are available for $f/f_{ce} > 0.25$. A comparison of the data from these two sweeps reveals that the transition from high to low values of θ occurs at different frequencies f, but approximately at the same normalized frequency f/f_{ce}: thus on sweep 1 the transition from $\theta = 72°$ to $\theta = 26°$ occurs between 1049 Hz and 1111 Hz, with $f/f_{ce} = 0.193$ on the average, while on sweep 2 the transition is from $\theta = 75°$ at 1494 Hz to $\theta = 22°$ at 1904 Hz, with an average $f/f_{ce} = 0.200$. On sweep 3, all the WDFs are at $f/f_{ce} < 0.2$, and their behavior is the same as that found at these low normalized frequencies on the previous two sweeps. The observation, on sweeps 1 and 2, of waves propagated at low θ values over a limited range of frequencies might be interpreted as the signature of cyclic waves; this possibility will be discussed in section 5.

In Figures 10 and 11 the more numerous data from passes III and IV have been presented slightly differently. The top, middle, and bottom of each figure contain the combined data from sweeps 1 and 2, from sweeps 3 and 4, and from sweeps 5 and 6, respectively; on pass III, it will be recalled, sweep 6 was incomplete. In most of the WDFs the θ values for the main peaks are clustered just below θ_G, while those for the secondary peaks extend lower, though rarely below 30° . Their distribution is much the same as it was on passes I and II in the same range of low normalized frequencies, notwithstanding that on passes III and IV the satellite was at relatively high magnetic latitudes.

4.2. ϕ Values

In trying to understand the ϕ values, we take the view that the variable f/f_{ce} is less important for ϕ than it is for θ but that the position of the satellite in relation to the source region is more important. This view is based on theoretical ray-tracing studies. It justifies our merging the data from all the different frequencies in each sweep, so as to improve the statistics. However, we have kept the data from the different frequency sweeps separate, as far as is practicable, since they refer to different ranges of L.

The data for passes I to IV appear in Figures 12 to 15, respectively. For each sweep of passes I and II, and for each pair of consecutive sweeps of passes III and IV, three histograms are presented: the first (checkered areas) gives the number of times that a primary peak was observed in each 20° interval; the second (hatched areas) gives the corresponding number for the secondary peaks; the third (solid line) gives the number of times that wave energy was observed in each interval at a level greater than 50% of the maximum value of the entire WDF. When studying these histograms it should be recalled that for $\phi = 0°$ the wave normal is in the local magnetic meridian plane and is directed downward (i.e., toward the Earth), for $\phi = 90°$ it is directed westward, and for $\phi = 180°$ it is again in the meridian plane but is directed upward.

First, let us examine the histograms for the occurrence of the peaks (checkered and hatched areas combined). From a synoptic view of all four figures, no general pattern emerges, but regularities are discernible for individual passes. On passes I and II, for instance, most of the histograms have two distinct peaks, which are close to the meridian plane on pass I but nearly perpendicular to it on pass II. The situation is more confused on passes III and IV, during which the histograms change as time goes on. This is particularly true for pass III, where the waves mostly have ϕ values close to 180° between $L \simeq 8$ and $L \simeq 6.6$ (sweeps 1–4) and then spread out as L decreases further. For pass IV, on the other hand, the distribution is relatively uniform at all L values. These last two passes covered overlapping ranges of L on the same day, so it seems that temporal as well as spatial changes were occurring, though one cannot be sure of this since the ranges of magnetic local time were different.

Now we turn our attention to the histograms for the range of ϕ over which the WDF exceeds half its absolute maximum value (solid lines). They are of particular interest for pass I, because this was the pass on which the satellite was closest to the magnetic equator (see Table 1). During the first two sweeps, most of the ϕ values lie in the interval $140° < \phi < 260°$, with a main peak varying from about 180° to 200° and a secondary peak between −40° and 40°. During the third sweep, two nearly equal peaks occur: the main one, which is quite wide, is centered around 200°; the second, also quite wide, occurs about 20°. During the fourth sweep, only small secondary peaks appear around 180°, while the main one is at 0°. Thus, on going from $L \simeq 4$ on sweep 2 to $L \simeq 2.5$

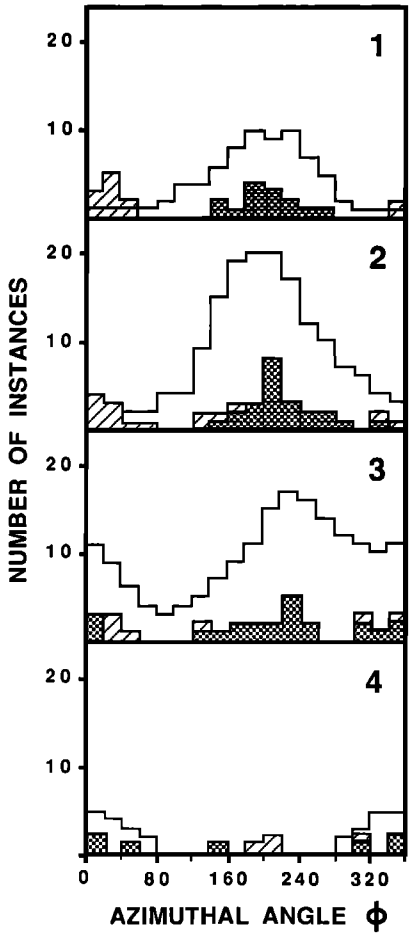

Fig. 12. Histograms of the azimuthal angle ϕ, in degrees, for the peaks of the WDFs, from the four successive frequency sweeps on pass I. See text for explanation.

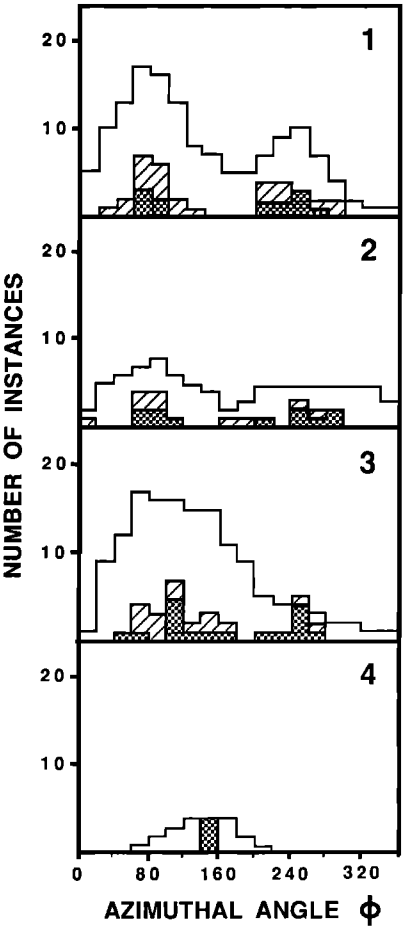

Fig. 13. Data similar to those of Figure 12, but for the four successive frequency sweeps on pass II.

on sweep 4, the direction of the main peak of the WDF, which is close to the meridian plane in both cases, changes in azimuth from being away from the Earth to being toward the Earth.

Although other explanations cannot be ruled out, such behavior is consistent with the view that most of the waves observed on this pass came from a broad source region, which extended over the positions of the satellite during sweeps 2-4 ($4.3 > L > 2.4$) and was most intense at the position during sweep 3 ($3.6 > L > 2.9$). This interpretation is supported by the following two facts: first, as already mentioned, there is an increase of the wave intensity on sweep 3; second, ray tracing shows that at the frequencies and L values concerned, waves generated in a source region on the equator and observed at low magnetic latitudes have their normals oriented upward ($\phi \simeq 180°$) at L values greater than that of the source and downward ($\phi \simeq 0°$) at smaller L values; at higher magnetic latitudes, however, the ray paths are less direct, and the situation is not so simple [*Cerisier*, 1970; *Burtis*, 1974; *Burtis and Helliwell*, 1976]. Thus the data suggest that the observed waves were being generated mainly below the satellite on sweep 2, all around it on sweep 3, and above it on sweep 4. More details as to how the two-peaked WDFs may be interpreted in terms of multipath propagation from a source region near the equator have been given by *Lefeuvre and Helliwell* [1985]; see also the paper by *Cairó and Lefeuvre* [1986], p. 4360 in particular.

In studying the data from pass II, which also was close to the equatorial plane, it is interesting to examine the ϕ values for the main WDF peaks that occur at low θ values in the range of $0.2 < f/f_{ce} < 0.3$ of normalized frequency on sweeps 1 and 2. For this purpose, the polar plot of Figure 16 shows the positions of the main peaks (solid circles) and of the secondary peaks (open circles) for all the WDFs

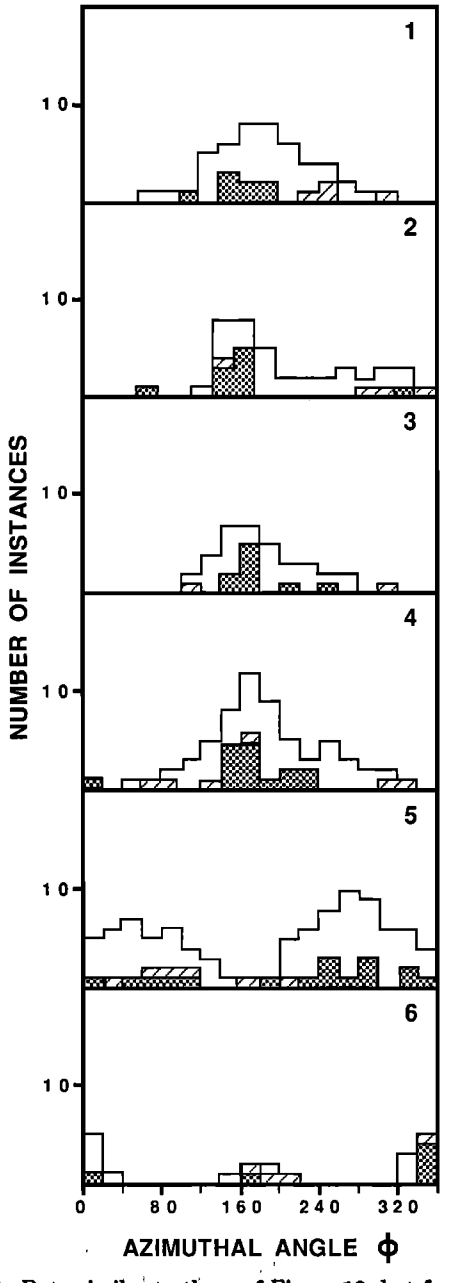

Fig. 14. Data similar to those of Figure 12, but for the six successive frequency sweeps on pass III.

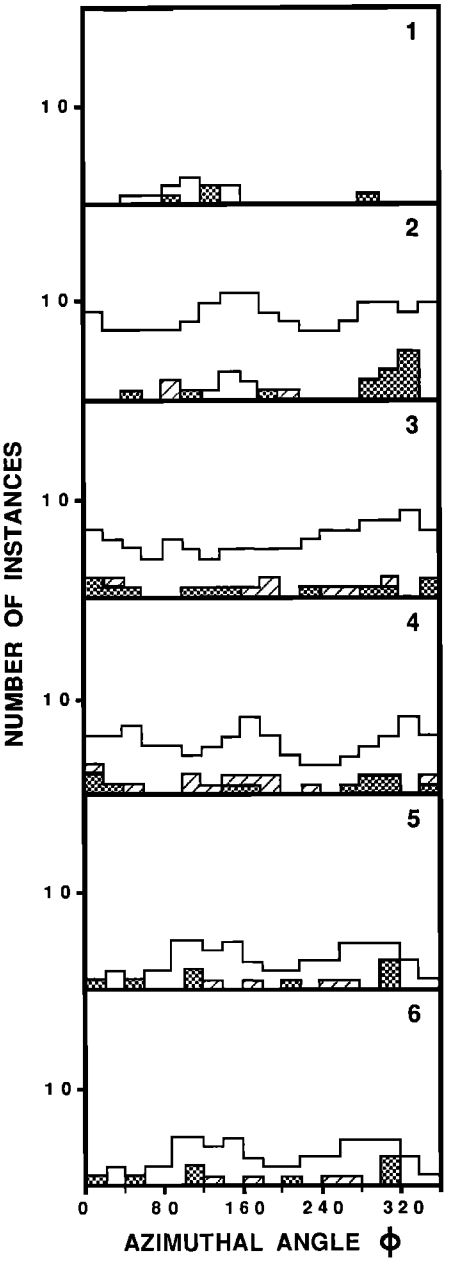

Fig. 15. Data similar to those of Figure 14, but for pass IV.

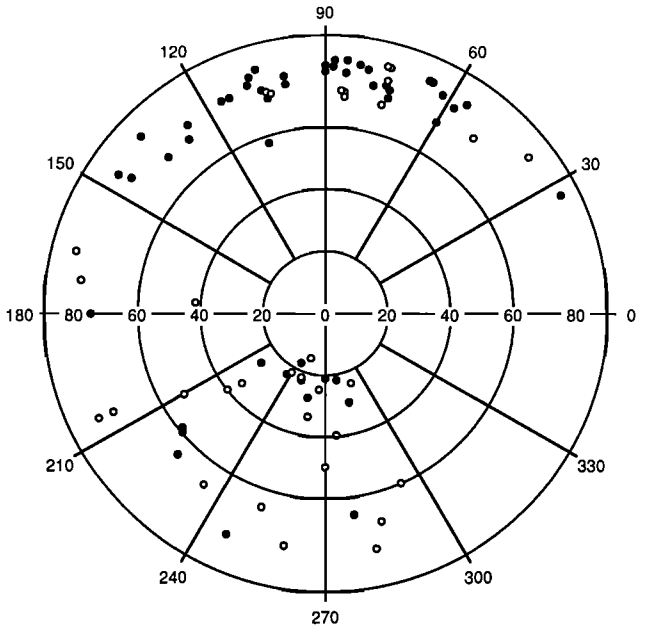

Fig. 16. Polar plot of the directions of the main peaks (solid circles) and secondary peaks (open circles) for all the WDFs from pass II.

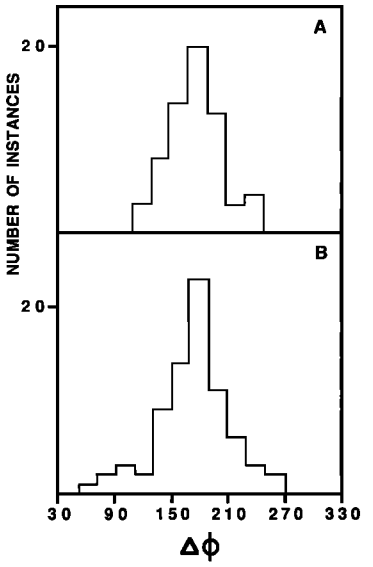

Fig. 17. Histograms of the difference, in degrees, between the azimuths of the main and secondary peaks, for all the two-peaked WDFs from (a) passes I and II and (b) passes III and IV.

obtained on this pass. Apparently all the low θ values, both those of the main peaks in the aforesaid frequency range and those of some secondary peaks outside this range, are associated with ϕ values between 200° and 300°. As regards the more numerous peaks at high θ values, some also occur between 200° and 300°, but most of them lie between 40° and 180°. Thus there is roughly 180° difference between the ϕ values for the WDF peaks at high and at low θ values.

This finding may be related to a general tendency that was found on all four passes, namely for the two-peaked WDFs to have their peaks at opposite azimuths. Figure 17 presents histograms of the difference between the ϕ values for the two peaks, the bin width again being 20°. Figure 17a contains the combined data from passes I and II, and Figure 17b contains those from passes III and IV. In both cases, the maximum of the histogram is at 180°; this tendency has been noticed previously in data from the GEOS satellites [*Lefeuvre and Helliwell*, 1985]. Neither the occurrence of two-peaked WDFs nor the statistics of $\Delta\phi$ appear to be related to the spatial position of the satellite with respect to the equatorial plane or to the plasmapause.

4.3. *Symmetry*

The overall symmetry of the WDFs is a further source of information as to whether the VLF waves observed on passes I and II were being generated, or at least amplified, at the L values at which they were observed, rather than being generated elsewhere and reaching these L values by propagation. The argument runs as follows. On the basis of previous theoretical models and experimental evidence, we assume that wave generation takes place mainly in a narrow range of low magnetic latitudes centered on the equator and that the generation mechanism is symmetrical about the equator, i.e., that equal wave energies are radiated from the source region into the northern and southern hemispheres. Subsequently the waves experience magnetospheric reflection and bounce back and forth between the two hemispheres while progressing to other L values. Therefore, if the waves are observed on or close to the magnetic equator at an L value where no generation is taking place, their true wave distribution functions $F(\omega_0, \cos\theta, \phi)$ should have reflection symmetry about the plane perpendicular to the Earth's magnetic field. This implies that the ambiguous wave distribution functions $\mathcal{F}(\omega_0, \cos\theta, \phi)$ as defined by (9), derived from the ELF magnetic field data alone, should have central symmetry about the direction of the Earth's field. On the other hand, at an L value where the waves are being amplified, at any point close to (but not exactly on) the magnetic equator, there is more wave energy coming out from the equator than going toward it, so here the ambiguous WDFs should not have this central symmetry. Observationally, while some of the WDFs for passes I and II do indeed have approximate central symmetry, lack of such symmetry is the norm; this is additional evidence that the ELF hiss waves are generated over a wide range of L values within the plasmasphere, and not merely just below the plasmapause.

At a point exactly on the equator, the WDFs should be symmetrical even at L values where the waves are being amplified. We checked this prediction, assuming the relevant equator to be the so-called "minimum-B" equator, where the component of ∇B_0 along the magnetic field lines vanishes [*Roederer et al.*, 1973]; its position was calculated using the Magsat 1980 model for the field, with the coefficients adjusted to the dates of the passes. On pass I, which lasted 63 min and spanned a range of 14.5° in magnetic latitude (see Table I), ISEE 1 crossed the minimum-B equator during frequency sweep 2, at 1442:40 UT. Out of the 53 WDFs made with the data from this pass, six were judged by eye to be approximately symmetrical, and three of them occurred around this time. The start times (UT) for the 32-s observing periods, and the corresponding frequencies, were as follows: 1441:27 at 1111 Hz; 1443:03 at 1299 Hz; and 1443:35 at 1494 Hz. The range of magnetic latitudes covered was roughly −0.2° to 0.3° with respect to the minimum-B equator. The WDFs for the second and third of these periods are shown respectively in Figures 5d

and 5e, respectively. However, between the first and the second there were two other periods, starting at 1441:59 (1173 Hz) and at 1442:31 (1235 Hz), for which the WDFs were less symmetrical. The other three symmetrical WDFS were observed at 1445:11 (3245 Hz), at 1455:18 (754 Hz), and at 1517:42 (1494 Hz). That three out of six were clustered around the estimated equator crossing time appears statistically significant, though not conclusive. This prediction about the symmetry of the WDFs should be checked again in the future, when larger and better data sets become available.

4.4. *Comparison With GEOS 1*

Before trying to explain our analyses of the plasmaspheric hiss observed by ISEE 1 and drawing conclusions, it is helpful to compare them with the corresponding results from GEOS 1, as reported by *Parrot and Lefeuvre* [1986]; this paper is referred to as PL below. GEOS 1, in an equatorial orbit, covered the range $4.5 \leq L \leq 9.9$. Hence it was only rarely inside the plasmasphere, and explored only the outermost parts of this region. The WDFs for plasmaspheric hiss observed by GEOS 1, like those from ISEE 1, often exhibit one or two distinct peaks.

The chief difference between the WDFs from the two spacecraft is that at magnetic latitudes below 10° and at normalized frequencies $f/f_{ce} < 0.2$ some of those from GEOS 1 have their main peaks at small θ values. Compare Figures 12 and 14 of PL with Figures 8 and 9 of the present paper. Only on pass II, and for $f/f_{ce} > 0.2$, did any of the WDFs from ISEE 1 have their main peaks below 30°. This difference may be linked to the fact that the GEOS 1 data were taken just below the plasmapause while most of the ISEE 1 data came from deep inside the plasmasphere.

On GEOS 1 many of the electric field data were exploitable, so it was possible to distinguish between waves propagating in opposite directions (see section 3.2). This ambiguity was resolved, in fact, for nearly half of the WDFs by estimating the parallel component of the averaged Poynting vector; this method can be applied only to WDFs with a single peak. Figures 15 and 20 of PL show that most of the waves observed by GEOS 1 at small θ values were propagating away from the equator, where they may have been generated or at least amplified.

5. RAY TRACING

Since the WDF analysis had revealed, on pass II, some cases of waves with their normal directions quite close to the magnetic field, a ray-tracing study was undertaken in order to find out whether these waves could possibly have been propagating on cyclic trajectories, as defined by *Thorne et al.* [1979].

For this purpose, models of the plasma and of the magnetic field were required. The basic plasma data were the variations of the plasma frequency f_p along the satellite orbit, which was quite close to the magnetic equatorial plane. They were scaled from Figure 2, in which f_p appears as the lower boundary of the grey area at the top of the spectrogram [*Gurnett et al.*, 1979]; the plasmapause can be seen at $L \simeq 8.2$. The measured points were smoothed by fitting a polynomial to the graph of $\log f_p$ versus L. Then the smoothed data were extrapolated to higher latitudes, assuming that the plasma was in thermal and diffusive equilibrium along the magnetic field lines, as in the model of *Angerami and Thomas* [1964], and that protons were the only ions present; the next most abundant ion, He^+, can be neglected because its proportion is usually in the range 2–6% [*Farrugia et al.*, 1989]. The variation of the plasma temperature across L shells was assumed to have followed the daytime model of *Geiss and Young* [1981]:

$$T(L) = T_1 - T_2/L \tag{10}$$

For T_1, which is the upper limit of temperature at large L, we took the value 1.152×10^4 K, and for T_2 we took 1.055×10^4 K. We used the centered dipole model of the Earth's magnetic field and neglected variations of the plasma density and temperature with geomagnetic longitude.

Our first ray tracings were made with the aim of discovering whether in the model plasmasphere defined above, cyclic or nearly cyclic trajectories could exist in the range of L (6.1–4.6) and of wave frequency f (1050–1900 Hz) in which waves with low θ values were observed on pass II. The procedure was to start a ray at the magnetic equator with the wave normal parallel to the field and to trace it until it either left the plasmasphere or returned to the equator with the normal pointing into the same hemisphere as at the start. In the latter case, the initial L value was changed slightly and the procedure repeated until either it became clear that no cyclic trajectories existed at the wave frequency concerned or such a trajectory was found. The results of this search were positive. One example of a cyclic trajectory, at $f = 1200$ Hz, is shown in Figure 18a; note that reflection occurs at the plasmapause even though the ray starts at a much smaller L value ($\simeq 4$). Other cyclic trajectories were discovered at lower frequencies, 800 Hz for instance (Figure 18b).

Nevertheless, it would be hazardous to conclude from these results that the waves observed near the equator on pass II with their normals at small θ values were propagating on cyclic trajectories. Their θ values, though small, were significantly different from zero, nor were these waves propagating in the meridian plane: their ϕ values were nearer to 90° or 270° than to 0° or 190° (see section 4). However, in order for the waves to be amplified repeatedly, every time they cross over the equator, it may not be necessary that they do so at the same magnetic longitude: it might suffice that they return to the equator at the same L value as at the start and with the same wave normal direction relative to the magnetic field.

Accordingly we made a search for this type of "quasi-cyclic" trajectory. Rays with the actual frequencies of observation were started at the equator, with θ values corresponding to the main peaks of the observed WDFs and with $\phi = 90°$. Once again, L was taken as an adjustable parameter; because of the uncertainties in our plasmaspheric model, we attached no great importance to the question of whether or not a ray starting from the actual point of observation, with the given initial conditions, would have a trajectory of this type. The ray tracings revealed that trajectories of the type sought for did indeed exist. Three examples are given in Figure 19. They correspond to three consecutive measurements made during the second WNA frequency sweep on pass II, when the satellite was at $L \simeq 4.8$. The figure presents the tracings in order of increasing frequency, which is also their chronological order, but it will be more convenient to discuss them in order of increasing θ value. The

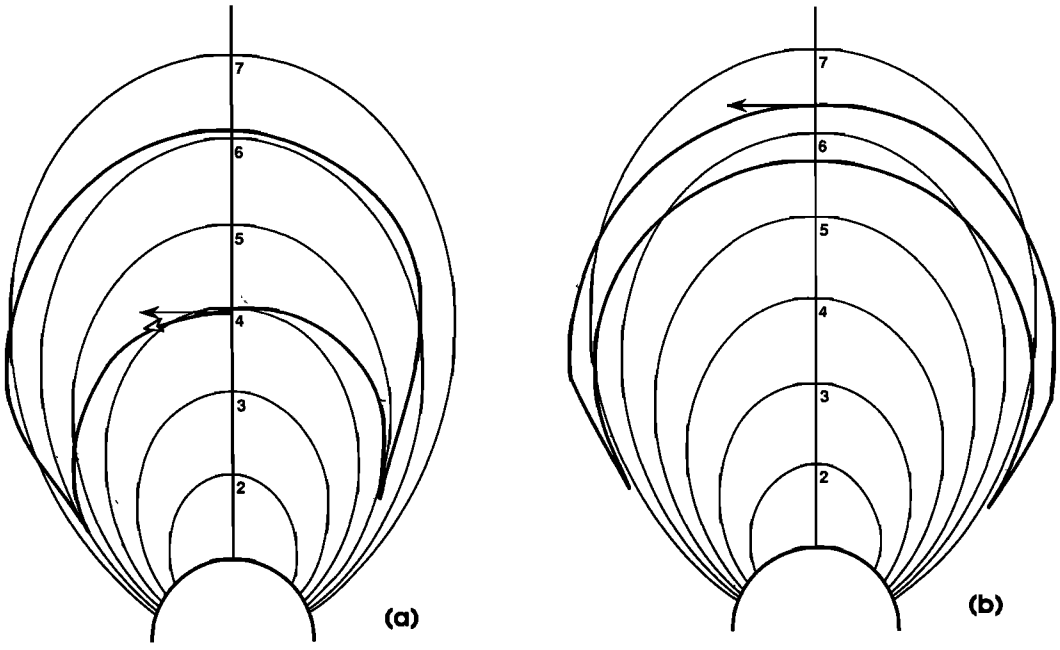

Fig. 18. Examples of cyclic trajectories in the magnetic meridian plane: (a) at 1200 Hz and (b) at 800 Hz. The arrows with the solid and open heads indicate the initial and final directions of the wave normal, respectively; in Figure 18b these two directions are almost the same. The magnetic field lines are shown at integer L values.

characteristics of the rays at the points where they cross the magnetic equator are summarized in Table 2.

Figure 19b shows a ray at 1904 Hz, which starts at $L = 3.72$ with $\theta = 22°$ and first returns to the equator at $L = 5.06$. Thus the upper and lower equatorial L values bracket the value of 4.8 at which the observations were made. The second crossing of the equator occurs close to the initial L value, though with a difference of 9.8° in longitude. However, the direction of the normal is no longer what it was initially: the angle θ has increased to 30°, and ϕ has gone from 90° to 182°, i.e., the normal is now almost in the meridian plane. Thus even when the change in longitude is discounted, the ray in this case is only approximately cyclic.

For the ray shown in Figure 19c, the frequency is 2195 Hz, the initial L value is 4.09, and the initial θ value is 30°. The first pass over the equator occurs at $L = 4.23$, which also is less than the observational value. On its second pass, the ray returns almost exactly to the initial L value, with its wave normal direction almost unchanged. The difference in longitude is 36.2°. This is a very good example of a cyclic ray, in our extended sense of the term.

Finally, the ray shown in Figure 19a was traced at 1695 Hz, starting from $L = 4.35$ with $\theta = 58°$. The first pass over the equator is at $L = 4.36$, and the second at $L = 4.35$ again. At this point where the tracing ends, θ has decreased to 42°, but ϕ is almost unchanged, so the ray is quite close to being cyclic.

A comparison of the three parts of Figure 19 reveals some general features of these quasi-cyclic rays that start with $\phi = 90°$ and nonzero θ. First, all of them are reflected well

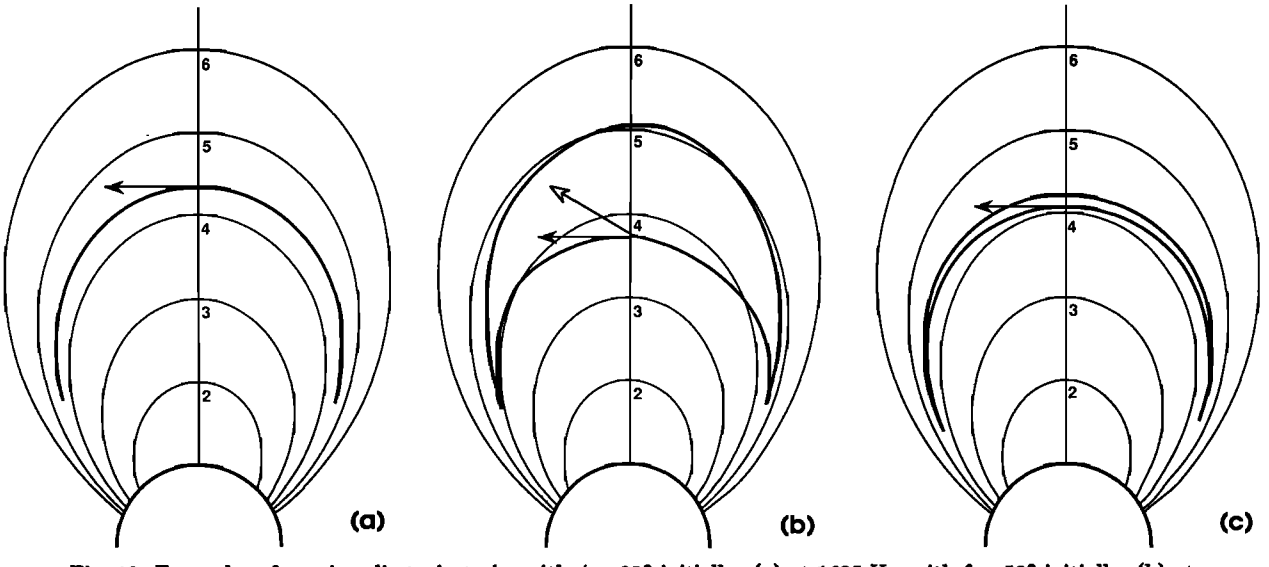

Fig. 19. Examples of quasi-cyclic trajectories with $\phi = 90°$ initially: (a) at 1695 Hz, with $\theta = 58°$ initially; (b) at 1904 Hz, with $\theta = 22°$ initially; and (c) at 2195 Hz, with $\theta = 30°$ initially. The solid and open arrows indicate the initial and final directions of the wave normal, respectively, projected onto the magnetic meridian plane.

TABLE 2. Characteristics of the Rays Traced in Figure 19, at the Points Where They Cross the Magnetic Equator

Figure	Frequency, Hz	L	θ	ϕ	Longitude
		Starting Point on the Equator			
19a	1695	4.35	58°	90°	0°
19b	1904	3.72	22°	90°	0°
19c	2195	4.09	30°	90°	0°
		First Pass Over the Equator			
19a	1695	4.36	130°	94°	−10.6°
19b	1904	5.06	136°	162°	−10.6°
19c	2195	4.23	149°	87°	−18.2°
		Second Pass Over the Equator			
19a	1695	4.35	42°	88°	0°
19b	1904	3.75	30°	182°	−9.8°
19c	2195	4.08	31°	90°	−36.2°

inside the plasmasphere, without ever reaching the plasmapause. This behavior contrasts with that of the rays shown in Figure 18, which, it will be recalled, were started with their normals parallel to the field. Second, increasing the initial θ value decreases the range of L values spanned by the ray, a tendency that is illustrated most dramatically by Figure 19a. *Church and Thorne* [1983] traced some quasi-cyclic rays starting with $\phi = 90°$ and $\theta = 30°$, but did not call attention to these features.

Let us extend the term "cyclic trajectories" or "cyclic rays" to cover what we have just now been calling quasi-cyclic trajectories. Henceforth we shall take it to refer to rays that return to their initial L values after two passes over the equator, and on which the waves have small equatorial θ values ($\leq 30°$, say) so that they are able to be amplified by the electron cyclotron instability.

In the light of the present ray-tracing study we conclude that at least some of the waves observed on pass II at small θ values may have been propagating on cyclic trajectories. However, it could be said of the waves observed on this pass at much greater equatorial θ values, which should not have been amplified, that their trajectories also may have returned to their initial L values. Indeed the same may very well be true of the waves observed on pass I at large θ values, close to the Gendrin angle, for this is the angle at which the trajectory follows a magnetic field line. In sum, the concept of cyclic trajectories does not help us to explain why waves were observed at low θ values at certain frequencies and not at others, nor why, in regions near the equator, waves at high θ values were by far the most common.

6. Discussion

From our WDF analysis of ISEE 1 data and from our ray-tracing studies, we find that cyclic waves may have played a minor role in generating the plasmaspheric hiss that we observed, but certainly not a major one. A salient feature of cyclic waves is that their normals are approximately parallel to the Earth's magnetic field at the equator, but for most of the hiss observed on the near-equatorial passes I and II this was not the case. Another of their features is that cyclic waves are reflected from the plasmapause, yet on passes III and IV much hiss was observed in the apparent absence of any distinct plasmapause. Hence, on these four occasions at least, it seems likely that most of the hiss must have been generated in some way not involving cyclic waves. These findings confirm and extend those presented by us in our earlier report [*Lefeuvre et al.*, 1983] and subsequently by *Hayakawa et al.* [1986b, 1987] and by *Sonwalkar and Inan* [1988].

Independent theoretical studies have led other workers to similar conclusions [*Huang*, 1981; *Huang and Goertz*, 1983; *Huang et al.*, 1983]. *Church and Thorne* [1983] also have revised their views on the significance of cyclic waves. Ray-tracing studies by Church and Thorne have shown that for a given model plasmasphere, cyclic waves can occur only in a few (three or four) discrete and narrow ranges of L; see, for example, Figure 9 of their paper. This prediction conflicts with the ISEE 1 observations of hiss spectra in the equatorial plane, as exemplified by Figure 14 of *Huang et al.* [1983] and by Figures 1 and 2 of the present paper.

The question therefore remains open of what other generation mechanism may be acting, and several new answers have been offered already. They all abandon one or more of three main postulates of the classical Kennel-Petschek theory, namely (1) amplification of the ELF waves by the whistler instability, on (2) trajectories that are in some sense cyclic, under (3) quasi-linear conditions.

If the prime source of wave energy is still assumed to be the Doppler-shifted electron cyclotron resonance (whistler) instability, but cyclic trajectories are not important, then one needs to know to what extent waves on noncyclic trajectories can be amplified before their normal directions become so oblique that amplification ceases. *Church and Thorne* [1983] considered waves recycled several times through the equatorial growth region on trajectories that internally reflect at the plasmapause but differ from cyclic trajectories inasmuch as they do not form closed loops and the wave normal directions are not exactly parallel to the magnetic field at the equator. They estimated the maximum amplification as 40 dB, while *Huang et al.* [1983], in a similar study but making less favorable assumptions, found only 4–5 dB. Even the higher figure, however, is much less than the 100 dB that would be required in order to produce hiss of the observed intensities from the natural incoherent emission. Accordingly *Church and Thorne* [1983] have proposed that hiss is produced by the amplification of waves from some as yet unidentified "embryonic source," these waves being initially at a level at least 60 dB above that of the

incoherent emission. As possible embryonic sources, they suggest chorus emissions, the low-frequency components of ducted whistlers, and auroral hiss. Assuming a smooth electron density distribution, their simulations show that near the equator the amplified waves should occur predominantly in a single roughly field-aligned cone. Most of our data show no such cone, so they are not consistent with this theory either.

Using particle as well as wave data from the GEOS 1 and GEOS 2 satellites, *Solomon et al.* [1988, 1989] have found cases where the measured distribution functions of the energetic electrons implied growth rates sufficient to amplify ELF waves from the thermal level to the observed hiss levels on a single pass through the magnetic equator, as had already been suggested by *Thorne et al.* [1979] and by *Cornilleau-Wehrlin et al.* [1985]. The data in question were taken when the satellite was near the equator and just below the plasmapause. *Solomon et al.* [1988] cite WDF analyses by *Parrot and Lefeuvre* [1986] showing that the waves observed at such points were propagating almost parallel to the magnetic field, in agreement with their theory. *Hayakawa et al.* [1987] have interpreted similar data as meaning that the waves were generated by the classical mechanism, but on trajectories guided by the plasmapause [*Inan and Bell*, 1977], which may be considered as special cases of the cyclic trajectories envisioned by *Thorne et al.* [1979].

These findings might be held to support the view of *Thorne et al.* [1973] that plasmaspheric hiss is mainly produced just inside the plasmapause and spreads out from there by propagation to fill the plasmasphere. However, it was partly to test this view that we chose, in preparing the present paper, to analyze data taken at times following long periods of magnetic quiet, when either there was no plasmapause or it was located unusually far from the Earth, at $L > 7$. Nonetheless, strong hiss was observed on all of the four satellite passes from which our data were taken. On passes I and II, where the satellite covered large ranges of L while remaining close to the magnetic equator, the upper cutoff frequency of the hiss increased steadily with decreasing L; at the lowest L values it was about 10 kHz (see Figures 1 and 2). Waves of these frequencies could not have originated just below the plasmapause, since the electron gyrofrequency, which is an upper limit for propagation in the whistler mode, is only about 2.5 kHz at $L = 7$. These observations imply that plasmaspheric hiss can be generated over a wide range of L values.

At the opposite extreme from the findings of *Solomon et al.* [1988, 1989], H. C. Koons (Private communication, 1984) has suggested that, at times, no amplification may be needed at all. Having noted that the increase of the cutoff frequency with decreasing L is consistent with propagation upward from a source at the bottom of the plasmasphere rather than downward from a source at the top, he suggested that plasmaspheric hiss might simply be the accumulated waves of many nonducted whistlers, all so highly dispersed that they have lost their coherent character. By ray tracing, taking account of the complex ionic composition of the topside ionosphere, *Kimura* [1966] and *Edgar* [1976] among others have shown that nonducted waves from lightning strokes at middle latitudes experience many successive magnetospheric reflections, at steadily increasing L values; this behavior is illustrated by Figure 20, which is a reproduction of Figure 9 of Edgar's paper. As the waves' upward

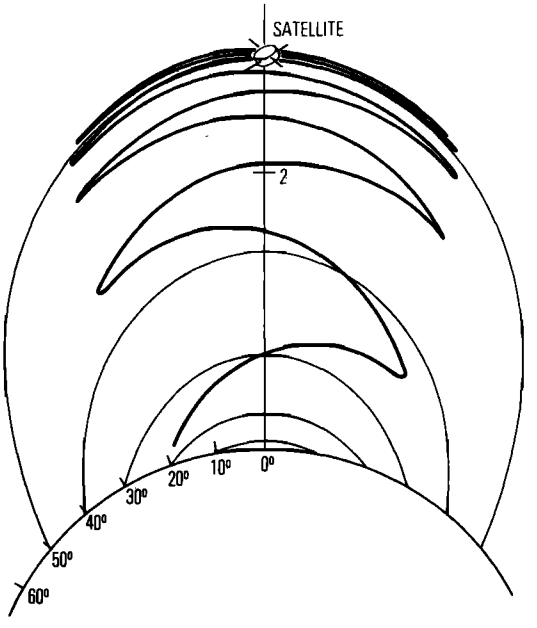

Fig. 20. Calculated ray path for waves at 1.75 kHz, staring from 18° magnetic latitude with the wave normal vertical [*Edgar*, 1976].

progress slows, their energy accumulates, so their intensity increases. In the limit, the waves shuttle back and forth across the equator, more or less on a fixed L shell, until ultimately they disappear by collisional and Landau damping. The suggestion is that plasmaspheric hiss consists of such waves, and indeed some of its properties, such as the obliquity of the wave normals, could be explained in this way. While this is debatable, the process invoked by Koons certainly takes place, and it provides an "embryonic source" of obliquely propagating waves for any instability capable of amplifying them, as *Sonwalkar and Inan* [1989] have pointed out.

This brings us to our own view, which is that the hiss waves observed by ISEE 1 near the magnetic equatorial plane were generated locally, approximately at the L values and at the wave normal angles at which they were observed. Indeed single-peaked WDFs (Figures 5a–5c), and also two-peaked WDFs that conspicuously lack reflection symmetry about the plane perpendicular to the magnetic field, are hard to explain in any other way. This hypothesis is consistent with the variations of hiss intensity and azimuth versus L observed on pass I, and with the observations on pass II of waves with large θ values and with $\phi \simeq 90°$ or 270° (Figure 16). The notion that nonducted whistler waves from lightning are an embryonic source of hiss is supported by a detail of Figure 1: the two horizontal bars near 11 kHz on the right-hand side of the figure are due to signals from ground-based transmitters of the Omega navigation network, and these signals are cut off at the same L values as the hiss. *Parrot* [1990] has surveyed the worldwide occurrence of natural emissions at three frequencies, using data from the AUREOL 3 satellite, and finds that regions of high thunderstorm activity are correlated with hiss at VLF (15 kHz and 4.5 kHz), though apparently not at ELF (800 Hz).

The main difficulty with this picture is to identify an instability capable of amplifying whistler mode waves at large wave normal angles under the conditions existing in the plas-

masphere. Several authors have discussed instabilities that can amplify oblique whistler mode waves [*Thorne*, 1968; *Young*, 1974; *Hashimoto and Kimura*, 1981], but in general the assumed electron distribution functions are inappropriate to the plasmasphere. *Parady* [1974] has discussed an anisotropic proton instability, whereby energetic protons in the ring current might also generate such waves, but this possibility has not been pursued by other authors, and we are not able to evaluate it.

An alternative is that the whistler instability might amplify oblique waves nonlinearly when they are sufficiently strong, under conditions where weaker oblique waves would be damped. It is well known that in experiments involving the transmission of VLF signals between ground stations at conjugate points the waves sometimes show little sign of being amplified at low intensities. Then, as soon as the intensity of the transmitted signals exceeds some threshold, the amplification increases greatly, and triggered emissions may occur, often resembling natural "chorus" emissions [*Helliwell et al.*, 1980]. The fact that chorus and hiss frequently occur together suggests that their generation mechanisms may be related [*Koons*, 1981; *Lefeuvre and Helliwell*, 1985]. However, these observations concern ducted waves, which propagate inside field-aligned irregularities with their normals more or less parallel to the field. The nonlinear process responsible for enhanced wave amplification, triggered emissions, and chorus is believed to be gyrophase trapping of cyclotron-resonant energetic electrons in the fields of ducted waves [*Helliwell and Inan*, 1982]. The fact that for longitudinally propagating whistler mode waves the plasma is more unstable in the nonlinear regime suggests that the same might be true for obliquely propagating waves, and indeed satellite observations of coherent VLF emissions triggered by nonducted waves give grounds for thinking that in the nonlinear regime the whistler instability can generate oblique waves [*Bell et al.*, 1981]. Whether an incoherent emission such as ELF hiss can be generated in this way is open to question, however, since broad-band incoherent waves are less apt than narrow-band coherent ones to cause gyrophase trapping.

Be that as it may, *Sonwalkar and Inan* [1989], using data from the DE 1 satellite, have recently reported observations of hiss emissions triggered by natural lightning-generated whistlers. They are triggered more often by oblique whistler waves than by longitudinal ones, and the resultant hiss waves also are found to be propagating obliquely. These observations, like our own, refer to magnetically quiet periods, with the daily average $K_p < 3$ on most days.

Even more recently, *Helliwell* [1989] has suggested that hiss may be generated by a nonlinear instability that should exist for broad-band whistler mode waves propagating close to the Gendrin angle [*Gendrin*, 1961]. His theory makes the interesting prediction that at L values where the distribution function of the energetic electrons is favorable there should be two zones of wave generation, one on either side of the equator, rather than a single one centered on the equator.

Predictions such as this could be tested most readily by WDF analysis of multicomponent wave data from polar-orbiting satellites. A single zone of wave generation at the equator could be identified unequivocally from the reversal that would occur in the predominant direction of the wave energy flux as the satellite crossed the equator; moreover, for those waves whose Poynting vectors were parallel or antiparallel to the orbital velocity vector, it should be possible to determine the spatial growth rate. On the other hand, if there were two zones, one on either side of the equator, the transition would be more gradual: in the space between the two, the north-going and south-going wave fluxes would be approximately equal. Finally, if the equator were crossed at a point where no waves were being generated, then the approximate equality of the north-going and south-going fluxes would persist over a broad range of latitudes on either side. For such studies it is vital that besides the three magnetic components of the wave fields, as many as possible of the three electric components should be measured as accurately as possible, so that the inferred WDFs are unambiguous.

7. CONCLUSIONS

The results presented above, taken with those published by previous experimenters, have led us to the following conclusions concerning the mode of origin of plasmaspheric hiss. The generation mechanisms proposed by *Kennel and Petschek* [1966], by *Thorne et al.* [1979], and by *Solomon et al.* [1988, 1989], among other authors, are all physically plausible and can come into action whenever the necessary conditions exist, in which case they give rise to waves that cross the magnetic equator with their normals at small angles to the magnetic field. However, hiss occurs even when the conditions for none of these mechanisms exist, and then it appears to be generated near the equatorial plane over a wide range of L values, with the wave normals at large angles to the field. The generation mechanism that applies in such cases is still unknown: multicomponent wave data from polar-orbiting satellites are needed to help identify it. The shortcomings of quasi-linear theory, together with the recent observations of hiss emissions triggered by whistlers [*Sonwalkar and Inan*, 1989], suggest that this mechanism may be nonlinear rather than quasi-linear.

Acknowledgments. The authors wish to thank J. G. Trotignon for providing information on the plasma frequency from the ISEE relaxation sounder experiment, and B. C. Edgar for supplying our Figure 20. We are grateful to H. E. Spence, R. J. Walker, D. P. Stern, G. A. Sacripanti, and Y. Ren for help in calculating the minimum-B equator for section 4.3. We thank D. L. Carpenter, R. A. Helliwell, U. S. Inan, and R. W. Burgess for their advice and comments. This work was supported in France by the Centre National d'Etudes Spatiales, which also provided computing assistance, and in the United States by National Science Foundation grant ATM-8318186 to Stanford University, by NASA grant NAG5-1093 to the University of Iowa, and by the award to one of us (L.R.O.S.) of a Senior Research Associateship from the National Research Council of the National Academy of Sciences.

The Editor thanks D. J. Gorney and R. A. Helliwell for their assistance in evaluating this paper.

REFERENCES

Aikyo, K., and T. Ondoh, Propagation of nonducted VLF waves in the vicinity of the plasmapause, *J. Radio Res. Lab. Jpn.*, *18*, 153, 1971.

Angerami, J. J., and J. O. Thomas, Studies of planetary atmospheres, 1, The distribution of electrons and ions in the Earth's exosphere, *J. Geophys. Res.*, *69*, 4537, 1964.

Bell, T. F., U. S. Inan, and R. A. Helliwell, Nonducted coherent VLF waves and associated triggered emissions observed on the ISEE 1 satellite, *J. Geophys. Res.*, *86*, 4049, 1981.

Bendat, J. S., and A. G. Piersol, *Random Data: Analysis and Measurement Procedures*, Wiley-Interscience, New York, 1971.

Burtis, W. J., Magnetospheric chorus, *Tech. Rep. 3469-3*, Radiosci. Lab., Stanford Univ., Stanford, Calif., 1974.

Burtis, W. J., and R. A. Helliwell, Magnetospheric chorus: Occurrence patterns and normalized frequency, *Planet. Space Sci., 24,* 1007, 1976.

Cairó, L., and F. Lefeuvre, Localization of sources of ELF/VLF hiss observed in the magnetosphere: Three-dimensional ray tracing, *J. Geophys. Res., 91,* 4352, 1986.

Cerisier, J. C., Propagation perpendiculaire au voisinage de la fréquence de la résonance hybride basse, in *Plasma Waves in Space and in the Laboratory,* vol. 2, edited by J. O. Thomas and B. J. Landmark, p. 487, Edinburgh University Press, Edinburgh, 1970.

Chan, K.-W., and R. E. Holzer, ELF hiss associated with plasma density enhancements in the outer magnetosphere, *J. Geophys. Res., 81,* 2267, 1976.

Chappell, C. R., Recent satellite measurements of the morphology and dynamics of the plasmasphere, *Rev. Geophys., 10,* 951, 1972.

Chappell, C. R., K. K. Harris, and G. W. Sharp, The morphology of the bulge region of the plasmasphere, *J. Geophys. Res., 75,* 3848, 1970.

Church, S. R., and R. M. Thorne, On the origin of plasmaspheric hiss: Ray path integrated amplification, *J. Geophys. Res., 88,* 7941, 1983.

Cornilleau-Wehrlin, N., R. Gendrin, F. Lefeuvre, M. Parrot, R. Grard, D. Jones, A. Bahnsen, E. Ungstrup, and W. Gibbons, VLF electromagnetic waves observed on board GEOS 1, *Space Sci. Rev., 22,* 371, 1979.

Cornilleau-Wehrlin, N., J. Solomon, A. Korth, and G. Kremser, Experimental study of the relationship between energetic electrons and ELF waves observed on board GEOS: A support to quasi-linear theory, *J. Geophys. Res., 90,* 4141, 1985.

Delannoy, C., and F. Lefeuvre, MAXENTWDF – A computer program for the maximum entropy estimation of a wave distribution function, *Comput. Phys. Commun., 40,* 389, 1986.

Dunckel, N., and R. A. Helliwell, Whistler mode emissions on the OGO 1 satellite, *J. Geophys. Res., 74,* 6371, 1969.

Edgar, B. C., The upper- and lower-frequency cutoffs of magnetospherically reflected whistlers, *J. Geophys. Res., 81,* 205, 1976.

Etcheto, J., R. Gendrin, J. Solomon, and R. Roux, A self-consistent theory of magnetospheric ELF hiss, *J. Geophys. Res., 78,* 8150, 1973.

Farrugia, C. J., D.T. Young, J. Geiss, and H. Balsiger, The composition, temperature, and density structure of cold ions in the quiet terrestrial plasmasphere: GEOS 1 results, *J. Geophys. Res., 94,* 11,865, 1989.

Geiss, J., and D. T. Young, Production and transport of O^{++} in the ionosphere and plasmasphere, *J. Geophys. Res., 86,* 4739, 1981.

Gendrin, R., Le guidage des whistlers par le champ magnétique, *Planet. Space Sci., 5,* 274, 1961.

Gorney, D. J., and R. M. Thorne, A comparative ray-trace study of whistler ducting processes in the Earth's plasmasphere, *Geophys. Res. Lett., 7,* 133, 1980.

Gurnett, D. A., F. L. Scarf, R. W. Fredricks, and E. J. Smith, The ISEE 1 and 2 plasma wave investigation, *IEEE Trans. Geosci. Electron., GE-16,* 225, 1978.

Gurnett, D. A., R. R. Anderson, F. L. Scarf, R. W. Fredricks, and E. J. Smith, Initial results from the ISEE 1 and 2 plasma wave investigation, *Space Sci. Rev., 23,* 103, 1979.

Harvey, C. C., J. Etcheto, Y. De Javel, R. Manning, and M. Petit, The ISEE electron density experiment, *IEEE Trans. Geosci. Electron., GE-16,* 231, 1978.

Harvey, C. C., J. Etcheto, and A. Manning, Early results from the ISEE electron density experiment, *Space Sci. Rev., 23,* 39, 1979.

Hashimoto, K., and I. Kimura, A generation mechanism of narrow-band hiss emissions above one half the electron cyclotron frequency in the outer magnetosphere, *J. Geophys. Res., 86,* 11,148, 1981.

Hayakawa, M., The generation mechanism of ELF hiss in detached plasma regions of the magnetosphere, as based on the direction finding results, *Mem. Natl. Inst. Polar Res. Spec. Issue Jpn., 47,* 173, 1987.

Hayakawa, M., N. Ohmi, M. Parrot, and F. Lefeuvre, Direction finding of ELF hiss emissions in a detached plasma region of the magnetosphere, *J. Geophys. Res., 91,* 135, 1986a.

Hayakawa, M., M. Parrot, and F. Lefeuvre, The wave normals of ELF hiss emissions observed on board GEOS 1 at the equatorial and off-equatorial regions of the plasmasphere, *J. Geophys. Res., 91,* 7899, 1986b.

Hayakawa, M., M. Parrot, and F. Lefeuvre, The wave distribution functions of plasmaspheric ELF hiss: GEOS 1 observation in the equatorial region, *Mem. Natl. Inst. Polar Res. Spec. Issue Jpn., 47,* 157, 1987.

Helliwell, R. A., *Whistlers and Related Ionospheric Phenemena,* Stanford University Press, Stanford, Calif., 1965.

Helliwell, R. A., Resonance interaction between energetic electrons and whistler mode waves at the Gendrin angle (abstract), *Eos Trans. AGU, 70,* 440, 1989.

Helliwell, R. A., and U. S. Inan, VLF wave growth and discrete emission triggering in the magnetosphere: A feedback model, *J. Geophys. Res., 87,* 3537, 1982.

Helliwell, R. A., D. L. Carpenter, and T. R. Miller, Power threshold for growth of coherent VLF signals in the magnetosphere, *J. Geophys. Res., 85,* 3360, 1980.

Huang, C. Y., A theoretical study of plasmaspheric hiss, Ph.D. thesis, Univ. of Iowa, Iowa City, 1981.

Huang, C. Y., and C. K. Goertz, Ray-tracing studies and path-integrated gains of ELF unducted whistler mode waves in the Earth's magnetosphere, *J. Geophys. Res., 88,* 6181, 1983.

Huang, C. Y., C. K. Goertz, and R. R. Anderson, A theoretical study of plasmaspheric hiss generation, *J. Geophys. Res., 88,* 7927, 1983.

Inan, U. S., and T. F. Bell, The plasmapause as a VLF wave guide, *J. Geophys. Res., 82,* 2819, 1977.

Kelley, M. C., B. T. Tsurutani, and F. S. Mozer, Properties of ELF electromagnetic waves in and above the Earth's ionosphere deduced from plasma wave experiments on the OV1-17 and Ogo 6 satellites, *J. Geophys. Res., 80,* 4603, 1975.

Kennel, C. F., and H. E. Petschek, Limit on stably trapped particle fluxes, *J. Geophys. Res., 71,* 1, 1966.

Kimura, I., Effects of ions on whistler-mode ray-tracing, *Radio Sci., 1,* 269, 1966.

Koons, H. C., The role of hiss in magnetospheric chorus emissions, *J. Geophys. Res., 86,* 6745, 1981.

Koons, H. C., Observations of large-amplitude whistler mode wave ducts in the outer plasmasphere, *J. Geophys. Res., 94,* 15,393, 1989.

Lefeuvre, F., and C. Delannoy, Analysis of random electromagnetic wave field by a maximum entropy method, *Ann. Telecommun., 34,* 304, 1979.

Lefeuvre, F., and R. A. Helliwell, Characterization of the sources of VLF hiss and chorus observed on GEOS 1, *J. Geophys. Res., 90,* 6419, 1985.

Lefeuvre, F., and L. R. O. Storey, The analysis of 6-component measurements of a random electromagnetic wave field in a magnetoplasma, 2, Model identification, *Tech. Note CRPE/41,* Cent. Natl. de la Rech. Sci., Cent. de Rech. en Phys. de l'Environ., Orléans, France, 1977.

Lefeuvre, F., M. Parrot, and C. Delannoy, Wave distribution functions estimation of VLF electromagnetic waves observed on board GEOS 1, *J. Geophys. Res., 86,* 2359, 1981.

Lefeuvre, F., T. Neubert, and M. Parrot, Wave normal direction and wave distribution functions for ground-based transmitter signals observed on GEOS 1, *J. Geophys. Res., 87,* 6203, 1982.

Lefeuvre, F., M. Parrot, L. R. O. Storey, and R. R. Anderson, Wave distribution functions for plasmaspheric hiss observed on board ISEE 1, *Tech. Note LPCE/6,* Cent. Natl. de la Rech. Sci., Lab. de Phys. et Chimie de l'Environ., Orléans, France, 1983.

Lyons, L. R., and D. J. Williams, *Quantitative Aspects of Magnetospheric Physics,* D. Reidel, Hingham, Mass., 1984.

McPherron, R. L., C. T. Russell, and P. J. Coleman, Fluctuating magnetic fields in the magnetosphere, 2, ULF waves, *Space Sci. Rev., 13,* 411, 1972.

Mosier, S. R., M. L. Kaiser, and L. W. Brown, Observations of noise bands associated with the upper hybrid resonance by the IMP 6 radio astronomy experiment, *J. Geophys. Res., 78,* 1673, 1973.

Muzzio, J. L. R., and J. J. Angerami, Ogo 4 observations of extremely low frequency hiss, *J. Geophys. Res., 77,* 1157, 1972.

Parady, B. K., Anisotropic proton instability magnetospheric (APIM) hiss: An introduction, *Geophys. Res. Lett., 1,* 235, 1974.

Parady, B. K., D. D. Eberlein, J. A. Marvin, W. W. L. Taylor, and L. J. Cahill, Jr., Plasmaspheric hiss observations in the evening and afternoon quadrants, *J. Geophys. Res., 80,* 2183, 1975.

Parrot, M., World map of ELF/VLF emissions as observed by a low-orbiting satellite, *Ann. Geophys., 8,* 135, 1990.

Parrot, M., and F. Lefeuvre, Statistical study of the propagation characteristics of ELF hiss observed on GEOS 1, inside and outside the plasmapause, *Ann. Geophys., Ser. A, 4,* 363, 1986.

Roederer, J. G., H. H. Hilton, and M. Schultz, Drift shell splitting by internal geomagnetic multipoles, *J. Geophys. Res., 78,* 133, 1973.

Russell, C. T., R. E. Holzer, and E. J. Smith, Observations of ELF noise in the magnetosphere, 1, Spatial extent and frequency of occurrence, *J. Geophys. Res., 74,* 755, 1969.

Russell, C. T., R. L. McPherron and P. J. Coleman, Fluctuating magnetic fields in the magnetosphere, 1, ELF and VLF fluctuations, *Space Sci. Rev., 12,* 810, 1972.

Samson, J. C., Matrix and Stokes vector representations of detectors for polarized waveforms: Theory, with some applications to teleseismic waves, *Geophys. J. R. Astron. Soc., 51,* 583, 1977.

Smith, R. L., Propagation characteristics of whistlers trapped in field-aligned columns of enhanced ionization, *J. Geophys. Res., 66,* 3699, 1961.

Smith, R. L., R. A. Helliwell, and I. W. Yabroff, A theory of trapping of whistlers in field-aligned columns of enhanced ionization, *J. Geophys. Res., 65,* 815, 1960.

Solomon, J., N. Cornilleau-Wehrlin, A. Korth, and G. Kremser, An experimental study of ELF/VLF hiss generation in the Earth's magnetosphere, *J. Geophys. Res., 93,* 1839, 1988.

Solomon, J., N. Cornilleau-Wehrlin, A. Korth, and G. Kremser, Generation of ELF electromagnetic waves and diffusion of energetic electrons in steady and non-steady state situations in the Earth's magnetosphere, in *Plasma Waves and Instabilities at Comets and in Magnetospheres, Geophys. Monogr. Ser.,* vol. 53, edited by B. T. Tsurutani and H. Oya, p. 119, AGU, Washington, D. C., 1989.

Sonwalkar, V. S., and U. S. Inan, Wave normal direction and spectral properties of whistler mode hiss observed on the DE 1 satellite, *J. Geophys. Res., 93,* 7493, 1988.

Sonwalkar, V. S., and U. S. Inan, Lightning as an embryonic source of VLF hiss, *J. Geophys. Res., 94,* 6986, 1989.

Storey, L. R. O., Radio sky mapping from satellites at very low frequencies, paper presented at URSI Commission E Symposium, Tokyo, Sept. 4–6, 1989.

Storey, L. R. O., and F. Lefeuvre, The analysis of 6-component measurements of a random electromagnetic wave field in a magnetoplasma, I, The direct problem, *Geophys. J. R. Astron. Soc., 56,* 255, 1979.

Storey, L. R. O., and F. Lefeuvre, The analysis of 6-component measurements of a random electromagnetic wave field in a magnetoplasma, II, The integration kernels, *Geophys. J. R. Astron. Soc., 62,* 173, 1980.

Taylor, H. A., H. C. Brinton, and A. R. Deshmukh, Observation of irregular structure in the thermal ion distribution in the duskside magnetosphere, *J. Geophys. Res., 75,* 2481, 1970.

Taylor, W. W. L., and D. A. Gurnett, Morphology of VLF emissions observed with the Injun 3 satellite, *J. Geophys. Res., 73,* 5615, 1968.

Thorne, R. M., Unducted whistler evidence for a secondary peak in the electron energy spectrum near 10 keV, *J. Geophys. Res., 73,* 4895, 1968.

Thorne, R. M., E. J. Smith, R. K. Burton, and R. E. Holzer, Plasmaspheric hiss, *J. Geophys. Res., 78,* 1581, 1973.

Thorne, R. M., S. R. Church, and D. J. Gorney, On the origin of plasmaspheric hiss: The importance of wave propagation and the plasmapause, *J. Geophys. Res., 84,* 5241, 1979.

Young, T. S. T., Electrostatic waves at half electron gyrofrequency, *J. Geophys. Res., 79,* 1985, 1974.

R. R. Anderson, Department of Physics and Astronomy, University of Iowa, Iowa City, IA 52242.

L. Cairó, Equipe de Recherche en Physique Mathématique, Modèlisation et Simulation, Centre National de la Recherche Scientifique, 3A Avenue de la Recherche Scientifique, 45071 Orléans Cedex 2, France.

F. Lefeuvre and M. Parrot, Laboratoire de Physique et Chimie de l'Environnement, Centre National de la Recherche Scientifique, 3A Avenue de la Recherche Scientifique, 45071 Orléans Cedex 2, France.

L. R. O. Storey, National Space Science Data Center, Code 930.2, NASA Goddard Space Flight Center, Greenbelt, MD 20771.

(Received November 5,1990;
revised June 20, 1991;
accepted June 20, 1991.)